



Glycerol-silica/chitosan conjugated self-assembled nano-flower framework for *Herstulla thompsoni* delivery with effectiveness in natural settings: Optimization and pilot scale production



Smriti Kala ^{a,*}, Chetan Jawle ^a, Mangesh AshokRao Pande ^a, Amrish Agarwal ^a, Krishna Kant ^b, B.K. Mishra ^b, Mukesh Kumar Singh ^a, L.K. Takhur ^a

^a Institute of Pesticide Formulation Technology (IPFT), Gurugram 122016, Haryana, India

^b National Research Center for Seed Spice Research, Ajmer 305206, India

ARTICLE INFO

Keywords:
Biopesticide
Chitosan
Herstulla thompsoni
Nano-flower gel
Self-assemble

ABSTRACT

Hirsutella thompsoni (HTS) is an entomopathogenic fungus (EPF), a secure and efficient substitute for synthetic insecticides. However, its susceptibility to degradation in conventional formulations limits its practical use for agricultural practices. In light of current setbacks, this work proposes using a glycerol-silica/chitosan nanoflower gel (NFG) as an efficient delivery system to enhance the efficacy of HTS. Inspired by glycerol-silica-chitosan conjugation, NFG self-assembles into flowers. The HTS-loaded nanoflower gel (HTS_NFG) features a flower-shaped morphology, an average size of 232 nm, and a zeta potential of +31.84mv. The laboratory-scale NFG is optimized with ingredients and process factors using multivariate principal component analysis (PCA), which progressed to pilot size 10 kg/shift. The notable foliage retention attributable to chitosan and lower contact angle was achievable on the hydrophobic leaf surface. The result of foliage retention and contact angle obtained showed a significant effect of NFG ($p < 0.05$). HTS_NFG was comparatively safer towards *Chlorella* spp. algae and *Artemia salina*, significant from other treatments ($p < 0.05$). Field efficacy evaluation demonstrated that the NFG was as effective as the reference sample against aphids. With its proven effectiveness, the NFG may be an aesthetic, sustainable, and feasible alternative for agro-production.

1. Introduction

The entomopathogenic fungus (EPF) has excellent potential for agricultural applications as an alternative to conventional chemical insecticides in sustainable pest management [1]. *Herstulla thompsoni* (HTS), a pathogenic fungus with numerous insect hosts, serves as widely employed as a biological control agent for field applications. Moreover, due to the potential adverse environmental and human health impacts, as well as the possibility of pest resistance development with the use of synthetic pesticides, EPF has been identified as a sound alternative management strategy against many insect pests, as a component of IPM approaches [2]. Microbial insecticides provide several advantages over conventional pest control products; yet their use in agricultural practices is not widely adopted. Environmental factors such as UV radiation significantly influence the efficacy of EPF-based pest control in field applications, making it less reliable than the chemical pesticides [3]. In

addition, several factors limit the microbial pesticide market, such as product quality control issues, including a low microbial count that results in poor performance in the field and a lack of large-scale production facilities [4].

The challenges of shelf life and efficacy of fungi-based bio-pesticides can be effectively resolved by an appropriate formulation; therefore, designing a suitable delivery system should aim to improve the shelf life of EPF. Among the currently available formulations, the WP (wettable powder) is most stable during storage, followed by WDG (water-dispersible granules) formulations. WP formulations have the disadvantage of dustiness; further, due to the dry-solid system, the shelf life in WP and WDG is compromised and not achievable as desired; therefore, fungi-based BPs face challenges under field conditions. In addition, conidia generated by EPF in liquid fermentations are more susceptible to experiencing reduced viability due to desiccation in solid systems such as WP and WDG [5]. In order to employ the entomopathogenic fungal

* Corresponding author at: Institute of Pesticide Formulation Technology (IPFT), Ministry of Chemicals & Fertilizers, Government of India, Gurugram 122016, Haryana, India.

E-mail address: smritikl16@gmail.com (S. Kala).

isolate as bio-pesticides, a substantial amount of spores is required. The successful growth of these spores depends on the substrate or medium, which is also crucial for effective formulation development [6]. The conidia produced by the fungus are extremely susceptible to many abiotic conditions, and using inappropriate substrates or media might result in a decrease in the quality and effectiveness of the conidia concentration [7], thereby reducing effectiveness of biopesticide. Furthermore, the of hazardous metabolites produced by EPF in formulated products, crops, and the environment, as well as their related risk is important to consider [8]. Therefore, a suitable delivery system with a simple preparation and EPF loading, optimum shelf life, non-target safety, and good foliar functionality that can meet the requirements of foliar efficacy is essential. Integrating bio-pesticides with suitable additives can produce a delivery system with high efficacy, increased shelf life, good adhesion performance, and low environmental impact [9].

In the recent work Sayed et al. [10] reported spray-dried formulation of microbial pesticides. *Bacillus thuringiensis* based formulation in combination with metallic nanoparticles have been reported by Patil et al., 2018 [11]. The current increase in commercial interest in microbial pesticides has resulted in improved and effective formulations. Still, their use as nanoparticles (NPs) for plant protection requires more investigation [12].

The nano suspension, which is stabilized by surfactants and prepared by a high-pressure homogenization process, has been considered a promising pesticide delivery system to overcome the problems of dispersion of pesticides, [13]. The particles dispersed into nano-suspension can be self-assembled into different shapes. Recently, there has been an increased interest in self-assembled polymer delivery systems such as nano-flowers. Nano-flowers are multi-morphology nano-structures made of polymers in aqueous media and are notable for their unique morphological properties, low cost of synthesis, and physico-chemical attributes like higher surface-to-volume ratios. According to Lee et al. (2022) [14], nanoflowers are primarily employed in biological applications and may be created using organic or inorganic materials or a mix of the two. The morphology of the nanostructures can also be affected by experimental parameters such as concentration, pH, and temperature [15]. Concurrently, it is possible to produce a stable nano flower gel (NFG) system by further processing the nano suspension system; this nano-system has enabled the practical application of many conventional pesticides [16].

Chitosan (CH), produced via the deacetylation of chitin, a natural polysaccharide sourced principally from crustacean shells, is a biopolymer with many commercial and biomedical uses [17–19]. CH has demonstrated the ability to produce eco-friendly and cost-effective organic-inorganic multifunctional-based nanocomposites for biological applications [20–22]. The exceptional biostability of CH has made it appropriate for the creating nanocomposites [23]. In addition, CH has been identified as an excellent rainfastness aid for a model agrochemical and viscofying agent [24,25]. The fumed silica [26] consists of a fundamental structure of branching patterns that enhance the roughness of the surface particles; in addition the presence of smooth particles on silica surface easily enables to commence the thickening process [26]. The CH and silica acts as rheology modifiers [27]. The amine and hydroxyl groups present in CH support the nucleation and the stabilization of suspension by preventing agglomeration and cluster formation [28]. The combination of silica and CH in the suspension initiates the thickening process, in a glycerol. The combination of glycerol-chitosan-silica increases viscosity, improving the stability and texture and also enhances the suspension's ability to suspend particles and prevent settling over time thereby stabilizes the suspension. Therefore, the combination of Silica and CH particles in the glycerol and water mixture also increase viscosity, making the suspension resistant to flow. This thickening effect is due to the intense attraction between the particles, resulting in a more structured flower shape [26].

Most research on the formulation technologies of pesticide is limited to laboratory optimization; scale-up to pilot plant still needs to be

explored. Since, the pilot-scale production from lab scale technology is the first step in developing large-scale production en route and commercialization and thus proving the technology's practicality and efficiency.

In view of the given background, this study aims to develop stable and effective formulation of EPF HTS for sustainable agricultural practices. HTS was suspended into glycerol using a wetting agent to produce a primary suspension, which has been subjected to high-pressure homogenization followed by conjugation with silica and CH producing nanoflower gel (NFG). Initially, the NFG was optimized considering ingredients and process parameters at a laboratory scale. We describe our efforts to produce pilot production (10Kg/shift). The characteristic features of NFG combined with silica-CH can significantly improve the exposed area of the carriers on leaf surfaces, increased shelf life, and efficacious performance, offers promising solution for efficient pest control. HTS has an effectively controls on various agricultural pests, however, the low resistance to environmental factors of HTS must be improved, to verify the feasibility of this strategy, we evaluate the insecticidal efficacy under field conditions.

2. Materials and methods

2.1. Materials

Glycerol and Propylene Glycol were purchased from Qualigens, Silica grade M-fill 100 was supplied by Madhu Silica and, methyl naphthalene sulphonate was supplied by Croda, Chitosan (High MW Degree of acetylation 75 %) (SRL chemical), HTS was supplied and identified by NRCSS, Ajmer India.

2.2. Design of experiment (DOE)

The critical process parameter affecting the product quality, like suspension stability attributes, was identified with an initial screening and optimization of selected non-ionic surfactants. We conducted a total of 15 trials using various input variables such as glycerol MNS ratio and stirring speed to prepare the primary suspension (coarse suspension), while maintaining a fixed ratio of propylene glycol and water. The response variable from various trials of suspensibility % was considered to select primary suspension (Table S1). Suspensibility was measured by the standard CIPAC method [29] (Supplementary text 1). The best primary suspension was further subjected to the process parameters like stirring speed, stirring time, homogenization time, and the number of homogenization cycles affecting the particle size were identified. A total of 12 trials were conducted with the different input variables to prepare nanosuspension (Table S2). The response variables from various trials, as well as their particle size, were considered when selecting nanosuspension. Finally, the silica and CH ratio was optimized based on viscosity to produce the final NFG from 9 trials.

2.3. Preparation of HTS-NFG

HTS_NFG was gel prepared as follows; initially, nanosuspension of HTS was produced in three steps; dispersion, followed by High-pressure homogenization [13] and addition of antisettling. The detailed steps are given below:

Step 1: Dispersion of MNS in water and propylene glycol: Primary suspension

The primary suspension was prepared following the previously described method with slight modifications [30]. Fixed concentrations of anionic surfactant (methyl naphthalene sulphonate), propylene glycol, and water were taken and thoroughly mixed.

Step 2: Addition of Glycerol and Dispersion of HTS

A glycerol ratio containing silicone defoamer (0.5 %) was introduced in the above mixture. HTS (5 mg) was macerated gently with a spatula and dispersed in the solution. The resultant mixture was mixed using a high-shear mixer (Silverson LM 5MA, England). The High shear mixer was operated at 5000 RPM for 5 min to ensure complete mixing of all ingredients and consistent HTS. The solution produced, thus, is named a coarse (primary) suspension of HTS.

Step 3: High-pressure homogenization - Particle size reduction of coarse suspension

The mixture produced in step 1 was homogenized using a High-pressure homogenizer (GEA Panda Plus, Italy) under different pressures in the range of 600 bars for five cycles per two minutes according to the previously described method with modification [31].

Step 4: Addition of silica-chitosan

The solution obtained from step 2 was further processed with (0.2 %) precipitated silica and (0.3 %) CH solution (1 % solution prepared in 0.1 % acetic acid) as an antisettler was added in two lots to avoid lumping. The solution was further subjected to the high shear mixer for 2 min (2000 rpm). Finally, the NFG of HTS was obtained.

2.4. Pilot scale production of HTS_NFG

The pilot scale production of HTS_NFG was accomplished at the Institute of Pesticide Formulation Technology (IPFT), Gurugram Pilot Plant facility. As per earlier optimized composition and process parameters from lab scale, the process was applied for producing 10Kg./shift in the Pilot Plant [31,32]. The batch process was carried out to produce HTS-NFG following a previous study. Similar steps were as for laboratory scale preparation was followed. The detailed Pilot scale production process and steps are given below:

1. Premixing step: Dispersion of MNS in water and propylene glycol

MNS was appropriately mixed with water, propylene glycol, and defoamer in a vessel to get a homogeneous solution in a shear mixer (1000RPM) following previously described method [13,31].

2. Addition of glycerol and dispersion of HTS

Glycerol and HTS biomass are charged into the vessel fitted with a high-shear mixer, and mixing is continued for 5 min to get homogeneous suspension at 5000 RPM.

3. High pressure homogenization

The suspension is charged into the HPH. The five cycles were given at 600 bar 2 min each. [31].

4. Addition of silica-chitosan for viscosity enhancement

Silica and CH (1 % solution prepared in 0.1 % acetic acid) were slowly added into the suspension with continuous high-shear mixing (2000 RPM), and mixing was done for 10 min to get the final product (HTS_NFG) [33].

The high-shear mixer equipment in the pilot plant is crucial for efficiently mixing and homogenizing the materials. It allows for precise control over the shear rate and ensures consistent product quality. The initial mixing took place in a stainless steel (SS) vessel. Temperature and pH control were achieved using two readers. The vessel was equipped with a stirrer, which was controlled by an electric motor set at a stirring speed of 1000 rpm. Water, MNS, and PG were suspended in the vessel to initiate the process. The temperature was set between 25 °C, and the

mixing proceeded for 5 min. The glycerol was introduced into the solution, followed by the addition of HTS and further mixing for 15 min. To homogenize the resultant solution, it was subjected to HPH at 600 bar 5 cycles per 2 min. The resulting solution was then mixed with silica-CH to produce HTS_NFG and stored at room temperature.

2.5. Characterization of laboratory scale and pilot scale batch

The particle size and zeta potential of NFG of both the lab scale batch and pilot scale batch were measured by the Brook Haven instrument (Nano Brook Zeta PALS). 100 mg/L sample solution was prepared in double distilled water, taken into transparent disposable polystyrene cuvettes, and measured size. Transmission electron microscopic (TEM) of lab scale batch and pilot scale analysis was carried out using a JEOL TEM 1011 microscope operating at 200 keV. The sample was ultrasonicated for 5 min [34]. The suspended NPs from NFG were loaded on carbon-coated copper grids (300 mesh). The sample containing grids were air dried for 30 min at room temperature before observation.

2.6. Rheology and FTIR

The flow behavior of the HTS_NFG laboratory scale batch was evaluated using a controlled shear rate rheometer (Anton Paar, Reolab QC, Austria) following Chu et al., 2015 [34]. HTS_NFG was carefully poured into the rheometer cup and allowed to stand for 2 min before shearing. Using a Peltier temperature device, the test temperature was set at 25 °C. The measurements, shear versus strain, were performed in the range of 0.1 to 100 1/s, and strain sweep measurement was conducted in the range of 0.01 to 100 % strain, and at a constant frequency of 10 rad/s, the storage (G') and loss (G'') moduli of the HTS_NFG was recorded. FTIR of laboratory scale batch was performed to study the insight of functional groups using an FTIR spectrometer (Burker Tensor 37, Germany) using ATR transmittance mode. Sixteen scans were obtained at a resolution of 4 cm⁻¹, from 4000 to 500 cm⁻¹.

2.7. Storage stability and degradable state

The degradable state of NFG was observed following the previously described method [35] with slight modifications. Sample of HTS_NFG was exposed to UV rays with an average irradiation intensity of 15 mW cm⁻² for 8 h and stored for 30 days at ambient temperature. The UV spectra and morphology of the HTS_NFG were observed after UV irradiation and after storage (30 days) and compared with freshly prepared samples. The particle size was also observed during a storage period of 30 days and compared with the initial particle size.

2.8. Wetting and spreading dynamics

The hydrophobic leaf of cabbage was used to assess the contact angle behavior of the HTS_NFG. The contact angles of the droplets were measured with a contact angle apparatus (Data Physics) following the previously described method [36]. The 5-µL diluted sample was dropped onto the leaf using a 50-µL syringe. The wetting spreading of the sample on the leaf was determined by the dipping method. The contact angle and droplet produced on the leaf surface were recorded and compared them with the reference sample. The contact angle behavior with drop age was also recorded. The spreading behavior was also assessed on leave; 1 µL of the sample was dropped on the leaf piece using a micro-pipette, and spreading behavior was recorded at different time intervals using a microscope (Nikon H 600 1 Japan); the dye was added for visualization. The thiamethoxam WDG (Thia-WG) was used as a reference sample.

2.9. Deposition property of the HTS_NFG on leaf surface

The foliage adhesion performance of HTS_NFG on hydrophobic

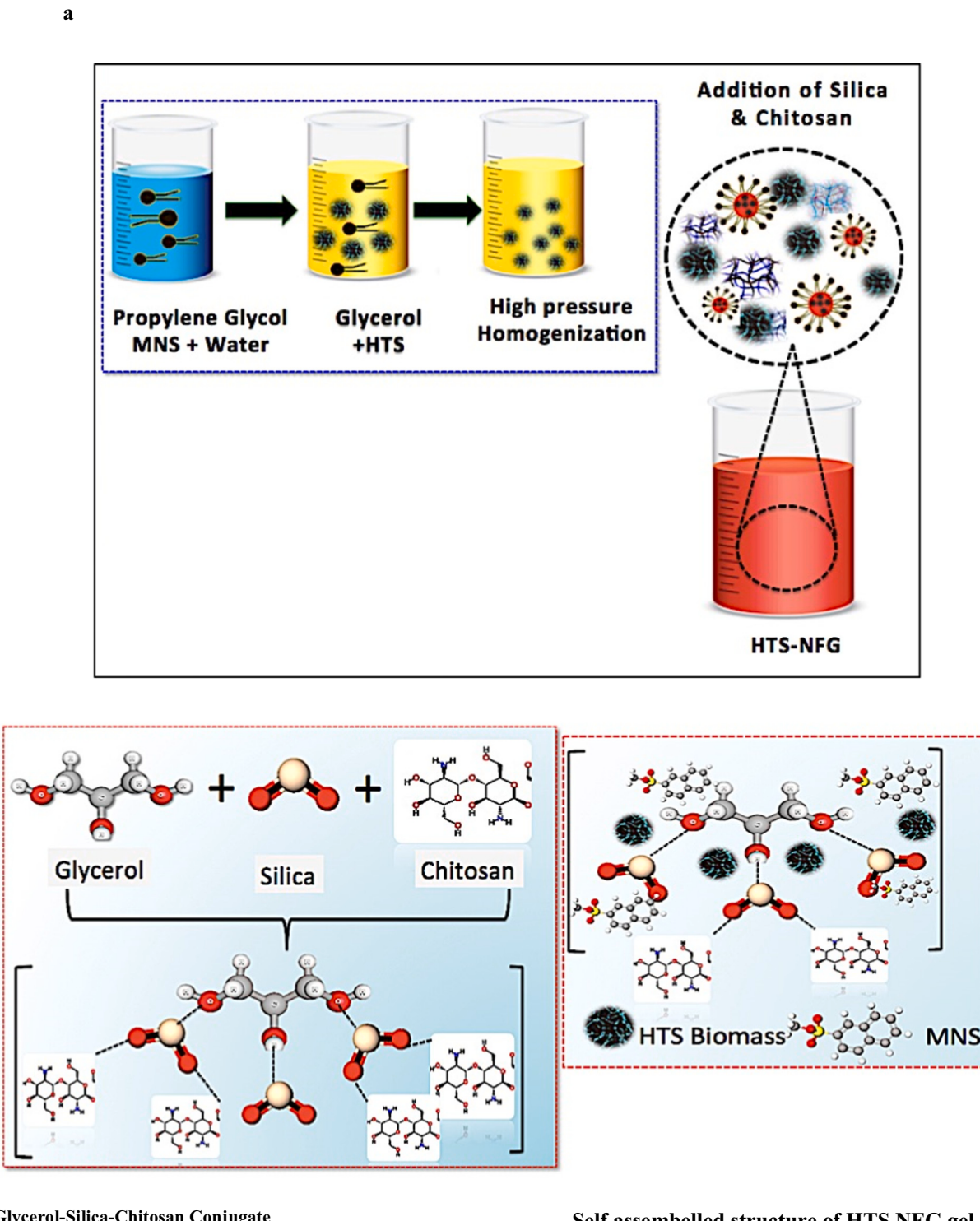
**Glycerol-Silica-Chitosan Conjugate****Self assembelld structure of HTS_NF gel**

Fig. 1. a) Illustration of preparation of HTS_NFG and Conjugation of glycerol -silica-chitosan and self assembled structure of HTS_NF Gel.

cabbage leaves was assessed using a previously reported method [37]. The spherical section of the leaf was cut, and the area (S) was measured; the leaf portions were then weighed. The HTS_NFG (diluted in water at 1 mg/mL HTS) was sprayed over the leaf portion at a 60-degree angle to the ground at a flow rate of 2 mL/min from a height of 20 cm for 10 min. The leaf portion weighed (W_1) was recorded after air-drying (20 min), and retention on a leaf (R_1) was computed using: mg/cm^2 .

$$R_1 = \frac{W_1}{S} \quad (1)$$

Subsequently, the leaf portions were repeatedly washed under running water for 15 min, followed by 20 min of air-drying. The leaf portions' weight was determined by (W_2) and retention on leaf was calculated by:

$$R_2 = \frac{W_2}{S} \quad (2)$$

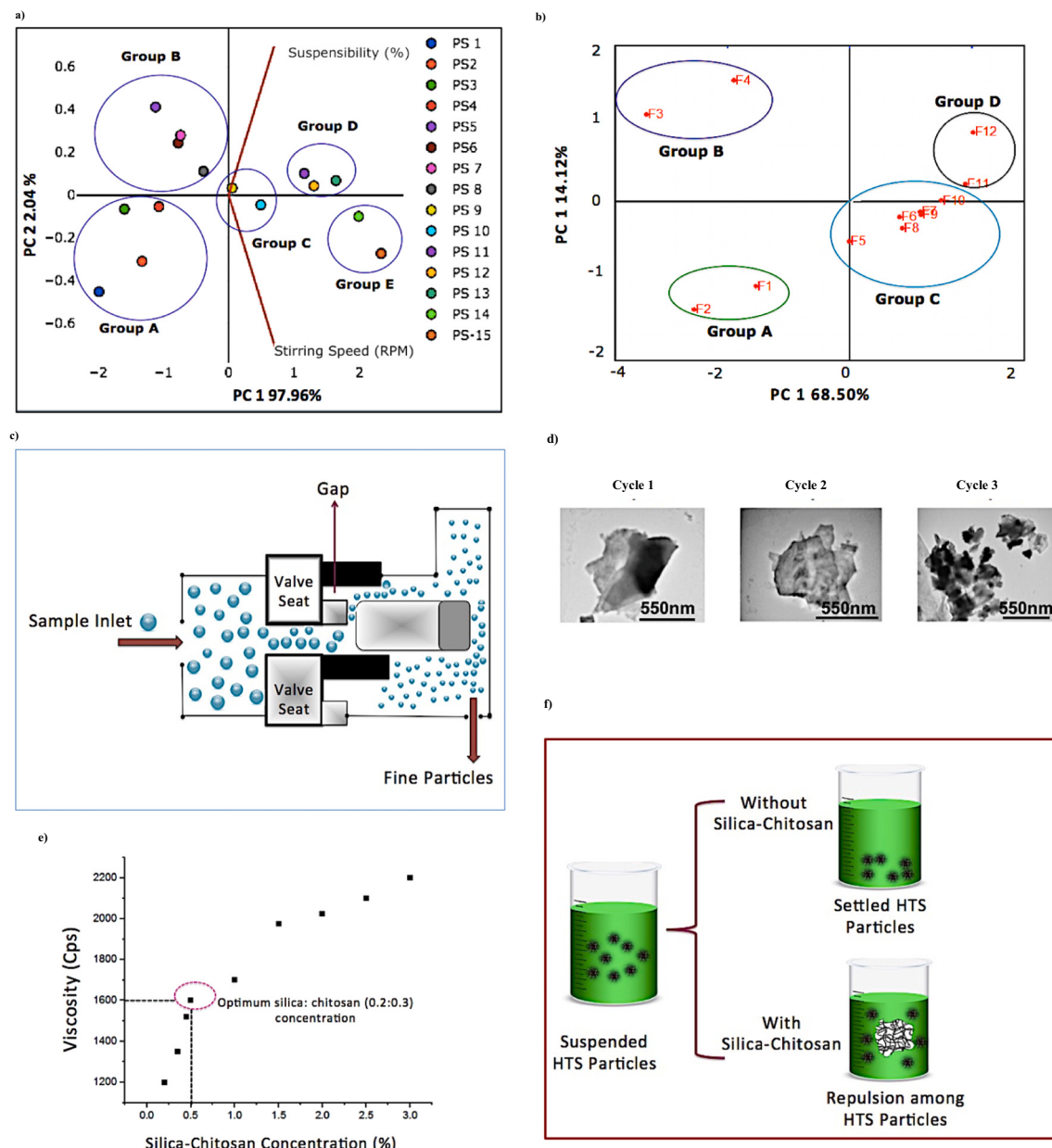


Fig. 2. a) Principle component regression analysis plot that depicts primary suspension (PS) correlation with surfactant concentration and stirring speed. b) Principle component regression analysis plot that depicts nanosuspension formulation (P) particle size correlation with high-pressure homogenization parameters. c) Mechanism of high-pressure homogenization (HPH). d) Change in morphology of HTS_NFG after different HPH cycles. e) Effect of silica: chitosan (0.2:0.3) concentration on viscosity of nanosuspension. f) Illustration of mechanism of HTS particles in presence of silica and chitosan.

$$\text{The loss - rate (LR)} \text{ was determined by } LR(\%) = \frac{R_1 - R_2}{R_1} \times 100. \quad (3)$$

SEM (FEI NOVA Nano SEM-450) was used to examine the surface morphologies of the leaves before and after washing.

2.10. Field bioassay of HTS_NFG

Crops of coriander (*Coriandrum sativum* L.) variety ACR-2 were sown in the end week of October 2021, while crops of cumin (*Cuminum cyminum* L.) variety GC-4 were planted on November 10th, 2021. All agronomic practices were performed following the method described by Kala et al., 2022 [38]. All treatments were tested on aphid populations that infested two spice crops. *Hyadaphis coriandri* was detected on coriander and fennel and *Aphis gossypii* was detected on cumin. All treatments were reproduced three times in 3×3 m² plots. The samples

were sprayed at (0.01 %).ai. ha⁻¹ with a spray volume of 400 L per hectare to ensure adequate coverage. The post-treatment observations on aphids were made from 5 leaves at the top, middle, and bottom of the plant. Populations were counted from 5 randomly selected plants per plot at 3, 6, and 9 days following spray. The control setup was without any treatment. The data was analyzed using RBD (Randomized block design).

2.11. Safety assessment on non-target

2.11.1. Bio-toxicity studies on micro-algae: growth kinetics and morphology alteration

Algal impacts through algae growth kinetics (protein measurement) were studied in *Chollera* sps. HTS_NFG, unformulated HTS, and Thia_WG in different treatments @ 100 µg/L. The concentration was prepared

within the BG-11 medium and was inoculated with algal inoculum (100 µg mL⁻¹ of protein value). The control was also taken without any treatment. Algal growth was evaluated based on protein quantification [39,40] using bovine serum albumin as standard, and absorbance of the samples was taken at 650 nm using UV-vis Spectrophotometer (Hitachi U2900). The protein content of treated cultures was measured at 5 days, 10 days, and 15 days. Scanning electron microscopy was used to analyze the surface morphology structure of cells exposed to HTS_NFG for 5 days. The treated algal cells were centrifuged at 1000 g for 5 min, air-dried them, and then imaged algal cells with FIE NOVA SEM.

2.11.2. Microcrustacean (*Artemia salina*) bioassay: acute and developmental toxicity

Artemia salina (Brine Shrimp) nauplii and cysts were obtained from a local supplier, kept in saline salt, and reared by the supplier guidelines. For the acute toxicity test the nauplii were maintained at 25 °C. For the developmental toxicity test the hatching procedure followed the ARC-Test method, and the artificial seawater of 35 g/L was used for the hatching as well as a testing solution [41]. Brine shrimp nauplii were obtained by hatching the cysts at 29 °C. For the acute toxicity test total of 10 Brine shrimp nauplii were exposed to the test solution (100.0 mg L⁻¹), prepared in the saline solution, at 25 ± 2 °C. All experiments were carried out in triplicate. At the end of exposure time (24 h, 48 h and 72 h), the number of organisms that survived was recorded. For the developmental toxicity study, the test concentration was prepared in saline water, *Artemia salina* cysts were carefully counted under a microscope approximately 5 No. of *Artemia* cysts were introduced in saline water under aeration at a temperature of 25 ± 1 °C. During the exposure period, abnormalities were observed under a phase contrast microscope (Nikon H 600 I Japan) at different time intervals, viz., 24, 48, and 72 h. The endpoints to assess developmental toxicity were abnormalities in the breaking stage, emerging embryos, and nauplii.

2.12. Seed germination potency assay

Seed germination potent assays of HTS_NFG were assayed by germination of cumin and coriander seeds and the emergence of plumules and radicles following previously described method [42]. The seeds were sterilized with 1 % aqueous NaOCl, then gently rinsed with sterile DDW 2–3 times; required samples as per MIC were applied in sterile filter paper. Filter paper that had been moist and sterilized was stored in a Petri dish, and sterilized seeds were then placed in the Petri dishes. After 72 h, the length of plumules and radicles was compared to control sets (no treatment).

2.13. Statistical and multivariate analysis

The relationships between the input design variables and response variables after primary suspension and nanosuspension were modeled with multivariate methods like principal component analysis (PCA) (Origin 10.5); formulation variables for primary suspension include stirring speed and ratio of glycerol: surfactant affecting suspensibility percentage, and for nanosuspension; stirring speed, stirring time, homogenization time, and number of homogenization cycle affecting the particle size were considered as input variables. The study presents the data as the mean of three replicates.

3. Results and discussion

3.1. Optimization of HTS-nanoflower gel formulation

The high-shear mixing and high-pressure homogenization (HPH) method has been employed to prepare HTS_NFG. Fig. 1a shows a flow-chart of HTS_NFG preparation and the formation of glycerol-silica-CH conjugate self-assembly. The high-shear mixing aids in the dispersion of the components uniformly, while the high-pressure homogenization

reduces particle size, achieving a more stable suspension and uniform particle size distribution, which is essential for consistent pesticide delivery performance. The anionic surfactant (methyl naphthalene sulphonate) has been selected to prepare NFG since non-ionic surfactants do not affect the pH and ionic strength of the solution [43]. The anionic surfactant stabilized the suspension and silica and CH, promoting self-assembly of the NFG. Overall, the study demonstrates that the combination of anionic surfactant, glycerol, silica, CH and high-pressure homogenization is essential for producing stabilized nanostructured flower gel. These findings provide valuable insights for further development and optimization of EPF delivery systems utilizing NFG technology.

3.1.1. Optimization of surfactant to produce primary suspension

Multivariate principal component analysis (PCA) was applied to different combinations of anionic surfactant and glycerol, whereas the aqueous phase and propylene glycol were kept constant. PCA classifies the sample pattern, grouping, similarities, and differences. Herein, the Glycerol: MNS ratio concentration and stirring speed were the input variables, and suspensibility was the output variable. The samples and variables located on the same side of principal components (PCs) are positively correlated, while those located on the opposite side of PCs show an inverse correlation. The present analysis explained 100 % variation in the data, the first PC with 97.96 % variations, and the second PC with 2.04 % variation. The PCA score plot (Fig. 2a) shows sample grouping, similarities, and differences. The PCA score plot showed five distinct groupings. Group A comprises primary suspension (PS) 1–4; Group B comprises PS 5–8; Group C PS9–10; and Group D PS 11–13; Group E comprises PS 14 and 15. These groupings in the PCA score plot are a function of the primary suspension's surfactant concentration, stirring speed, and resulting property, i.e., suspensibility %. Group A showed a negative correlation with primary suspension, stirring speed, and MNS concentration along PC1 and PC2; this indicated that these formulations containing a low amount of surfactant had a lower suspensibility. The groups B, C, and D had a positive correlation with PC2. On the other hand, Group E PS exhibited positive correlations with stirring speed and surfactant concentration along PC2. Group E PS showed an inverse relationship with Group A formulations along PC1. Thus, Group E formulations contained high surfactant and underwent high shear rates, producing higher suspensibility than Group A formulations. Consequently, Group E PS has a high suspensibility due to the high amount of surfactant and high shear mix. The results showed that the combination of surfactant and glycerol had the highest impact on the variance in the suspensibility data and a direct relationship between the suspensibility percentage with surfactant concentration and stirring speed. This can be attributed to the enhanced sorption of MNS at the water interface, which leads to the infringement and good dispersion of fungal biomass. The increase in the concentration of MNS beyond a certain limit, saturation occurred, and no more increase in suspensibility rate was observed. This saturation point indicates an optimal ratio of MNS to glycerol for achieving maximum suspensibility. Further studies could explore different surfactants or additives to enhance the suspensibility of HTS potentially.

3.1.2. Optimization of HPH process parameters for nanosuspension

Multivariate principal component analysis (PCA) was applied to the number of homogenization cycles, and homogenization time as input variables and suspensibility and particle size as output variables (Table S2). The PCA analysis explains 82.62 % variation in the data, the first PC with 68.5 %, and the second PC with 14.12 % of the variations (Fig. 2b). The PCA score plot showed four distinct groupings. Group A comprises F 1–2; Group B comprises F 3–4; Group C F5–10, and Group D F 11–12. The F11 and F12 are positively correlated along PC1 and PC2. These results indicated that these formulations have small particle size due to more excellent homogenization time and cycles. The PCA analysis revealed a clear separation between the four groups based on their resultant particle sizes. The positive correlation of F11 and F12 along

Table 1

Details of composition and experimental conditions for Pilot Production of HTS_NFG (MOC = Material of construction; SS = stainless steel; VFD = Variable frequency drive panel; HP = Horse Power).

Composition				
S. No.	Material	% W/V	Quantities in ml (for 10 kg. batch)	
1.	D.M Water	5–10	500–1000 (0.5 kg–1 kg.)	
2.	Propylene Glycol (PG)	5	500 (0.5 kg.)	
3.	MNS-90	2–7	200–700	
4.	HTS Biomass	1.5	150	
5.	Glycerol	84.5	8450 (8.45 kg.)	
6.	Silica: chitosan	5 (0.2:0.3)	200–500 10,000 g. (10 Kg.)	
Total		100		

Process parameters				
Stages and equipment	Temperature	Mixing time	Stirring RPM/pressure	Equipment specs.
Premixer: Premixing of PG+MNS+Water	25 °C	5 min	1000RPM	1. Capacity: 25 L 2. Stirring assembly: Fitted with geared motor & VFD 3. Motor: 0.5HP 4. MOC = SS 304
Charging of glycerol to premix solution	25 °C	5 min	1000RPM	1. Capacity: 25 L 2. Stirring assembly: Fitted with geared motor & VFD 3. Motor: 1 HP 4. MOC = SS 304
High Shear Mixer: Addition of HTS Biomass	25 °C	15 min	5000RPM	1. Capacity: 25 L 2. Stirring assembly: Fitted with geared motor & VFD 3. Motor: 1 HP 4. MOC = SS 304
High Pressure Homogenization		5 cycles per 2 min	600 bar	
Addition of Silica & chitosan	25 °C	10 min	2000RPM for 5 min	

PC1 and PC2 suggests that these formulations have undergone required transformations in terms of particle size through the homogenization processes. PCA graph shows that F12 lies at a distinct height than F11; consequently, F12 has the lowest particle size, which can be attributed to the high homogenization cycle and time.

The critical property of nanosuspension (NS) is the particle size, as this property indicates the feature of the formulated nanosuspension, and it is a direct reflection of the process parameters of the suspension, which is demonstrated through PCA. The HPH method used to develop the suspension offers various benefits, including the absence of organic solvents, lower energy consumption during milling, and more feasibility [31]. High-pressure homogenization (HPH) is a purely mechanical process, which is evoked by forcing a fluidic product through a narrow gap (the homogenizing nozzle) at a high pressure (Fig. 2c). The HTS primary suspension, when passed through the homogenizing nozzle at high pressure ranging between 600 bars at very high shear, stress occurs, which produces very fine droplets of suspension. The optimized ingredients of suspension and process parameters, like high-speed shearing mixing speed (3000 rpm) and HPH (600 bars, five cycles for 2 min), might favor the dispersion, stabilization, and self-assembly of HTS particles producing nanosuspension (NS). The change in morphology of PS after different HPH cycles is presented in Fig. 2d.

3.1.3. Optimization of silica-chitosan concentration and self-assembly into nanoflower

The silica-CH ratio was selected as a possible viscosity modifier; the ratio of silica-CH was optimized based on the viscosity measurements at different concentrations (Fig. 2e). When silica was used alone, the settling of HTS biomass was observed; therefore different silica-CH ratios were investigated. The results of viscosity measurements of different combinations of silica and chitosan viz. 0.5 % (0.2) + CH (0.3), 1 % (0.5:0.5), 1.5 %(1:0.5), 2.0 % (1:1), 2.5 %(2:0.5), and 3 %(2.5:0:0.5) indicated that HTS nanosuspension with 0.5 % viscosity modifiers combination as silica (0.2) + CH (0.3) provided optimum viscosity of 1600 cP. Beyond 0.5 % (0.2) + CH (0.3) silica: CH concentration in the range of 1 % (0.5:0.5), 1.5 %(1:0.5), 2.0 % (1:1), 2.5 %(2:0.5), the suspension became viscose, and at concentration 3 % (2.5:0:0.5) it leads to a dense solution with visible silica particles. The suspension of NFG produced with 0.5 % silica-CH (0.2:0.3) was homogeneous and had minimal visibility of silica particles. The results of viscosity measurements indicate that a concentration of 0.5 % silica-CH may be optimal for producing NFG.

The optimum concentration of viscosity modifiers like silica and CH is critical in creating a more stable formulation as it offers the stable dispersion of the pesticide particles (HTS Biomass) by providing a barrier. The extremely low silica: CH concentration may induce HTS biomass sedimentation, whereas the high amount may promote increased viscosity. When evaluating the relative performances of silica: CH, the 0.5 % silica: CH yielded the best results and hence was chosen for creating the final NFG. When introduced into glycerol, the strong intermolecular forces between the silica particles and the viscosity-enhancing nature of CH [16] create a network-like structure bearing a flower shape. An illustration of the mechanism of HTS particles in the presence of silica and CH is presented in Fig. 2f.

3.2. Pilot scale production

The process, conditions, and equipment used in the pilot plant production of HTS_NFG are given in Table 1 and Fig. 3a, b, respectively, following which the pilot batch of 10Kg/shift was successfully produced (Fig. S1 a). The pilot batch was similar to the laboratory batch in appearance; upon characterization, it was observed that the pilot batch had a particle size (241 ± 38 nm), zeta potential of +31.48mv, and flower shaped morphology, which was similar to the laboratory batch. (The parameters are discussed in the detailed characterization section.) Thus, the consistent results (of three important parameters, i.e. particle size, zeta potential, and morphology) of the lab batch and pilot ensure that the manufacturing process is reproducible across different scales, which is crucial for ensuring product quality and performance. Most of the previous research on nanomaterials and biopesticides is restricted to laboratory optimization; however, the pilot-scale production is the initial step towards large-scale production and commercialization and is critical for verifying the technology's viability and efficiency.

3.2.1. Self-assembly mechanism of HTS_NFG formation

The self-assembly of HTS_NFG in a glycerol/silica-CH mixture with the addition of water and a non-ionic surfactant was found to be highly influenced by the addition of each ingredient, including surfactant, silica, and chitosan, resulting in the formation of unique flower shaped nanostructures. The addition of surfactant, silica, and CH played a crucial role in controlling the morphology and size of the nanostructures formed during self-assembly. In prior study, it was found that both CH and silica serve as rheology modifiers and the presence of amine and hydroxyl groups in CH facilitates the stabilization of suspension by inhibiting agglomeration and cluster formation creating self assembly [27,28]. The self-assembly process was carried out using two different batch sizes: laboratory scale and pilot scale. The results revealed that the combination of silica and CH in a glycerol/surfactant/water/HTS solution forms a self-assembled flower framework. Fig. 3c illustrates the

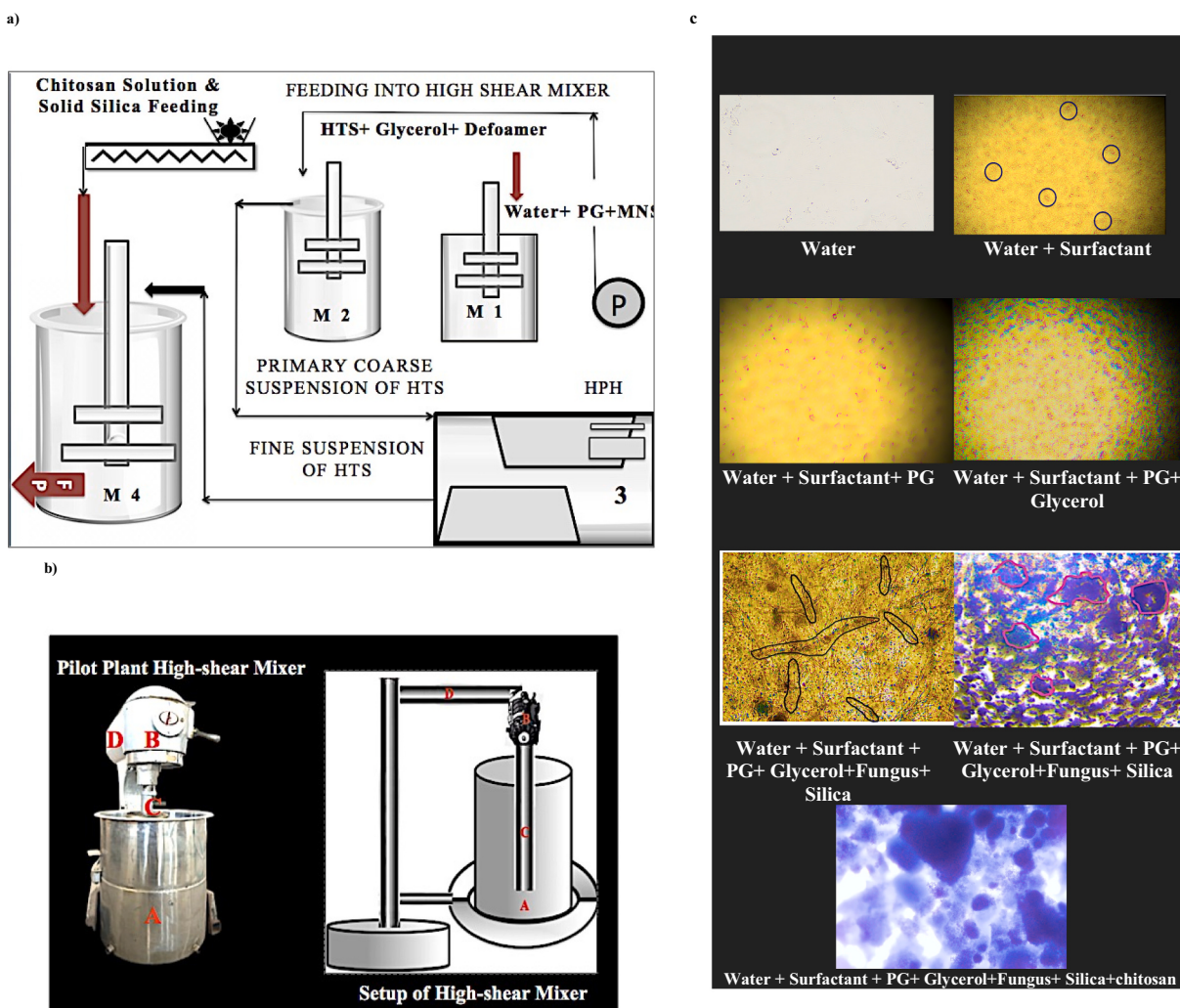


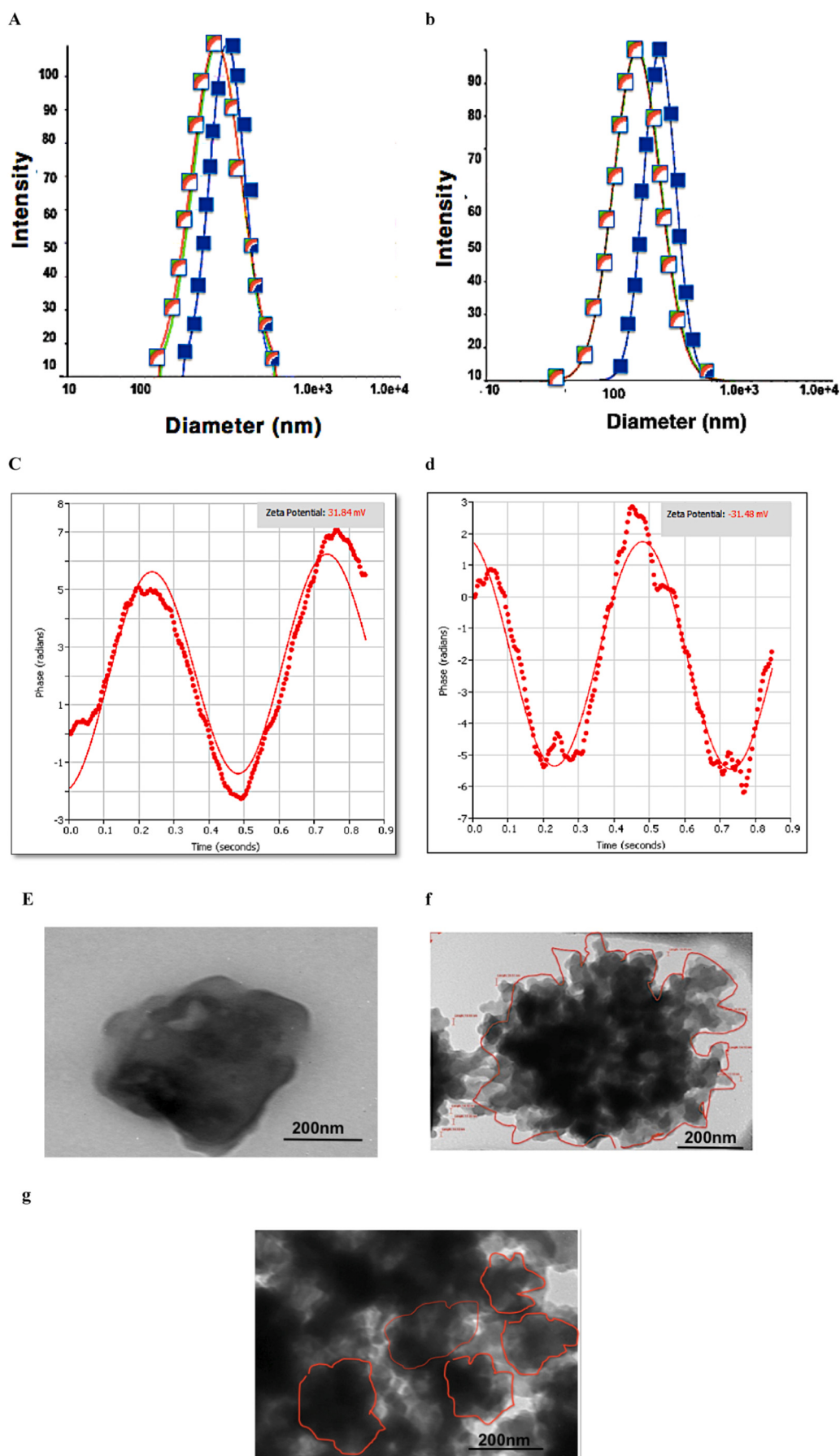
Fig. 3. a) Design and lay out for Production of HTS Suspension (1 = Mixing Tank; 2 = High shear Mixer; 3 = High pressure Homogenizer; 4 = Final Product Mixer; FP = Final Product HTS_NFG; M = Motor; p = pump) b) High Shear Mixer setup used for pilot Scale production of HTS_NFG: (A—Vessel; B—Blade Motor; C—Stirrer; D—Metallic Stand). c) Self-assembly mechanism of HTS_NFG formation: Optical microscope images of changes in morphology after addition of each ingredient. (Blue round circle = surfactant aggregate in water; Black line fungus (HTS) mycelia; red line aggregates in flower shape forming HTS_NFG (Magnification 10×). (For interpretation of the references to colour in this figure legend, the reader is referred to the web version of this article.)

morphology of the water system, including surfactant (MNS-90), propylene glycol, and glycerol. Following the introduction of HTS, the presence of mycelia in the system is readily apparent. After the introduction of silica, and the addition of CH to the solution, a rearrangement occurs, forming nanoflower gel (NFG), the structure of the flower shape becomes more distinct after adding CH. The underlying mechanism of nanoflower gel assembly may be attributed to the framework of fumed silica and CH, which readily initiates the thickening process and generates clusters through enhanced particle interactions facilitated by their unique structure and properties. The thickening effect and eventual self-assembly result from the robust attraction between the particles, leading to a more organized flower structure. Therefore, it can be inferred that the self-assembly of nanoflower gel (NFG) in the system is caused by the clustering properties of silica and CH in the presence of glycerol and other ingredients, resulting in the development of nanoflower.

3.3. Characterization of laboratory scale and pilot scale batch

The primary particle size of the laboratory and pilot scale batch, as determined by DLS, was 232 ± 24 nm and 241 ± 38 nm, respectively (Fig. 4a, b). The zeta potential of the laboratory batch and pilot scale

batch HTS_NFG was $+31.84$ mv and 31.48 mv (Fig. 4c, d). Zeta potential is a useful parameter for evaluating the stability of colloidal systems [44]. The surface charge of the particles can control their strength in the formulation, leading to a strong electrostatic repulsion between them [44]. The morphology of the HTS mass and HTS-NFG of both batches was imaged by TEM; the fungus before loading to NFG appears to be a bulk mass without any defined structure, shape, and assembly (Fig. 4e), whereas HTS_NFG from both the laboratory and lab scale batch was observed with a noticeable interlinked assembly possessing a uniform structure and flower shapes. (Fig. 4f, g). The observed variations in morphology between HTS and HTS_NFG may be attributed to factors such as processing method, optimized surfactant concentration, and the application of a viscosity modifier, silica-CH with glycerol, which facilitates the self-assembly of HTS biomass into NFG structures [27,28]. The results show a likely change in the morphology of HTS biomass after loading into NFG, suggesting a uniform flower shape connection between HTS and NFG. The uniformity of morphology is crucial for enhancing the interaction between the core material and the surrounding matrix. In addition, the three important parameters of nano-material i.e., Particle size, Zeta potential, and morphology of the laboratory and pilot batch were almost similar; the results of the comparison of the three parameters suggest that the manufacturing process



(caption on next page)

Fig. 4. a) DLS of HTS_NFG laboratory batch (3 replicates) b) DLS of HTS_NFG pilot scale batch (3 replicates) c) Zeta potential of laboratory batch d) Zeta potential of pilot scale batch (where red dotted line for sample red line for standard) e) Morphology of unprocessed HTS fungal mass before formulating. f) TEM micrograph of laboratory scale NFG g) TEM micrograph of pilot scale NFG showing fungus after conjugation between glycerol and silica and self-assembled with MNS attaining flower shape (HTS_NFG) red out line used for defining flower shape. (For interpretation of the references to colour in this figure legend, the reader is referred to the web version of this article.)

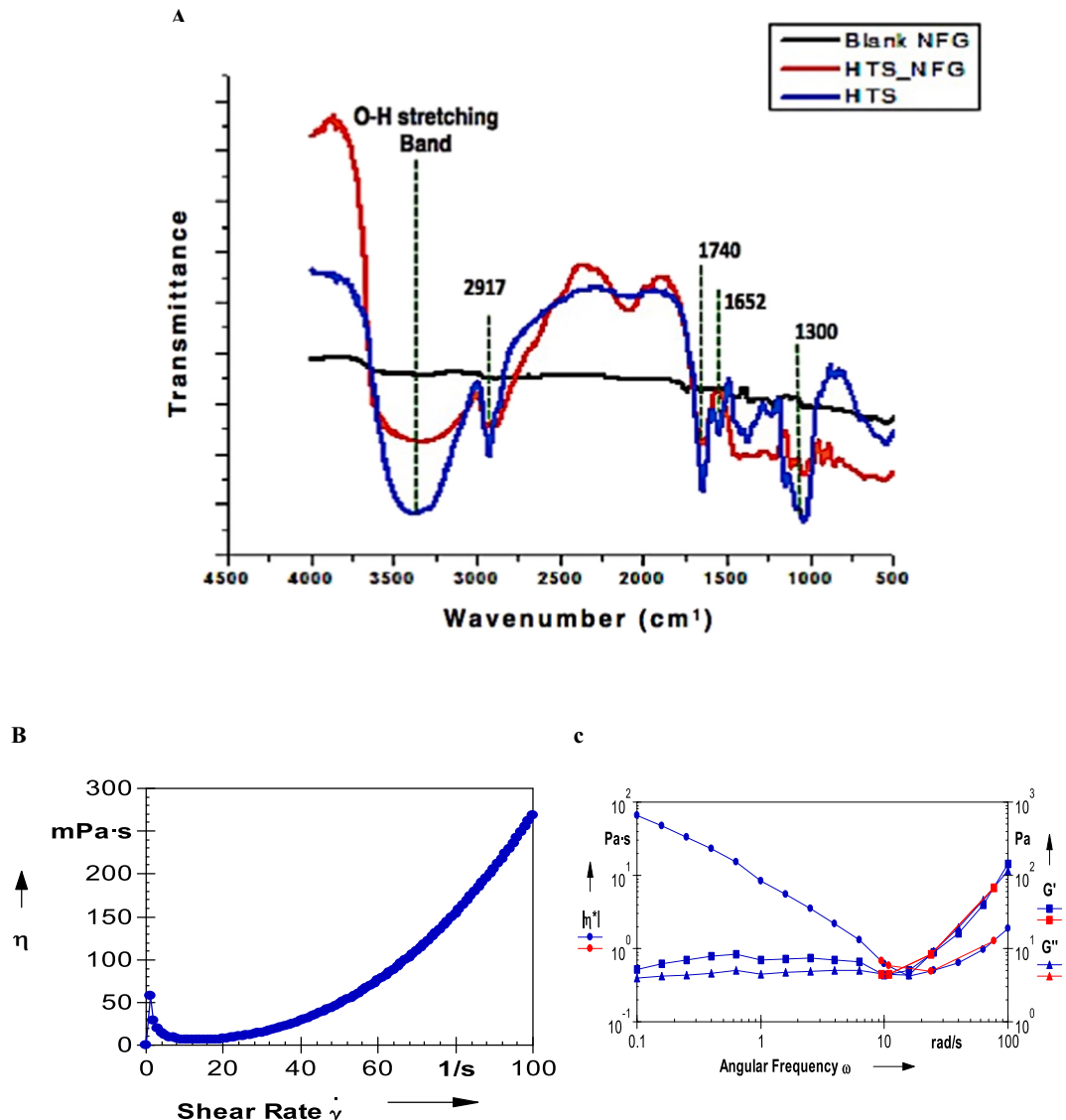


Fig. 5. a) FTIR spectra (1 = HTS; 2 = HTS_NFG; 3 = Blank NFG). Rheological properties of HTS_NS (Laboratory batch) b) Viscosity as a function of shear c) Frequency dependence of storage modulus, G' , loss modulus, G'' , and complex viscosity, η^* .

is consistent and reproducible across different production scales, which indicates that the product quality and performance were consistent. Therefore, other characterizations were preceded by the laboratory batch.

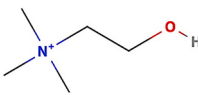
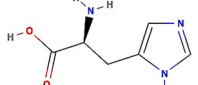
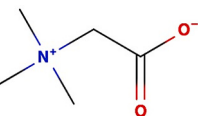
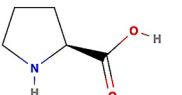
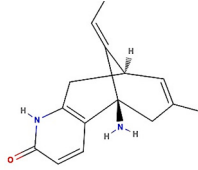
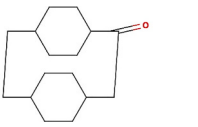
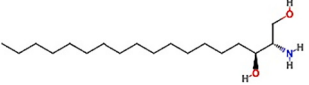
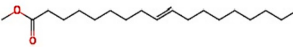
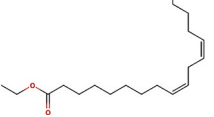
3.4. Functional groups and compatibility study (FTIR) and NMR characterization

The functional group and interaction analysis of HTS_NFG was carried out using FTIR. Fig. 5a shows a typical infrared absorption spectrum for EPF_HTS and HTS-loaded NFG. The lower region of the spectrum has a peak at 1150 cm^{-1} , mainly due to the vibration of carbohydrate and nucleic acids, peak at 1300 cm^{-1} due to amino acids, 1652 cm^{-1} and 1740 cm^{-1} attributable to the amides and lipids, respectively [45]. In the upper

wavenumbers region of the spectrum, bands at 2849 cm^{-1} and 2917 cm^{-1} are dominated, mainly due to lipids [46,47]. FTIR characterization suggests the presence of carbohydrates at 1150 cm^{-1} , nucleic acid vibrations at 1300 cm^{-1} , amine at 1652 cm^{-1} , and amide at 1740 cm^{-1} are altered in NFG compared to unformulated HTS. The bonding of HTS to NFG through the bands at 2849 cm^{-1} and 2917 cm^{-1} due to lipid absorbance environments is also reflected as shifts in the regions. The independent FTIR spectra of propylene glycol; Surfactant (MNS-90); glycerol, CH, and silica are given in Fig. S1 b. Comparing the spectra of HTS_NFG, HTS with other components (propylene glycol; Surfactant (MNS-90); glycerol, CH and silica, a broad peak pattern of the hydroxyl group ($-OH$) appeared at around 3200 cm^{-1} to 3500 cm^{-1} in HTS-NFG, were found to be suppressed compared to the blank NFG, and also to the other components (propylene glycol; Surfactant (MNS-90); glycerol,

Table. 2

Major metabolites of HTS.

Name of metabolite produced by HTS	Structure	Chemical nature	Toxicity data
Choline		Amino acid	Low toxicity on Brine shrimp, Zebra fish and Green algae [50,66]
Histidine		Amino acid	-
Betaine		Modified Amino acid	-
Proline		Proteinogenic amino acid	-
Huperzine A			
P-Cyclophane		Hydrocarbon Containing aromatic unit	No toxicity against three microalgae, [52,62,67]
Safingol		Lyso-sphingolipid protein kinase inhibitor.	-
Methyl elaidate		Fatty acid methyl ester	-
Ethyl linoleate		Fatty acid Ethyl ester	-

CH and silica). The presence of HTS in NFG leads to a shift in the region between 1100cm¹ and 2900cm¹ due to the successful loading of HTS into NFG, Kumar et al., 2018 reported shift in peak of FTIR spectra after loading of active [48]. The ¹³C NMR and ¹H NMR spectra of NFG before blank NFG are shown in supplementary fig. 1c and supplementary text-3. The shift in peaks of NMR spectra in blank NFG and HTS-NFG confirmed that molecular arrangements might occur after loading HTS in NFG, leading to self-assembled flower structure. This structural change is evident in the differences observed between the two spectra, indicating a molecular rearrangement led to the formation of a self-assembled flower structure.

3.5. Rheological behavior of HTS_NFG

The rheological properties of a formulation are crucial for controlling and facilitating the appropriate dispersion of the pesticide during spray

applications. Rheology study is therefore as effective method to examine the flow-related characteristics of formulation by assessing the impact of the shear rate on the viscosity of formulation. The applied shear rate has an impact on the viscosity of HTS_NFG (Fig. 5b). As the shear rate increases, the viscosity of HTS_NFG also increases, leading to a continuous increase in viscosity; this behavior aligns with the rheological properties of dilatant and shear thickening fluids (STF). In this study, a nano-suspension carrier was developed where nanoparticles were made from HTS, and anionic surfactant self-assembly, which was spread out evenly in a continuous glycerol medium, followed by subsequent addition of silica and CH to the mixture. Under moderate shear rates, the nanoparticles may deform readily, but at high shear rates, they immediately undergoes transition to a highly viscous state due to release of the impact force; this is supported by previous research [49,50]. The NFG carrier exhibited similar shear thickening behavior, demonstrating their potential during spray applications. The findings suggest that NFG could

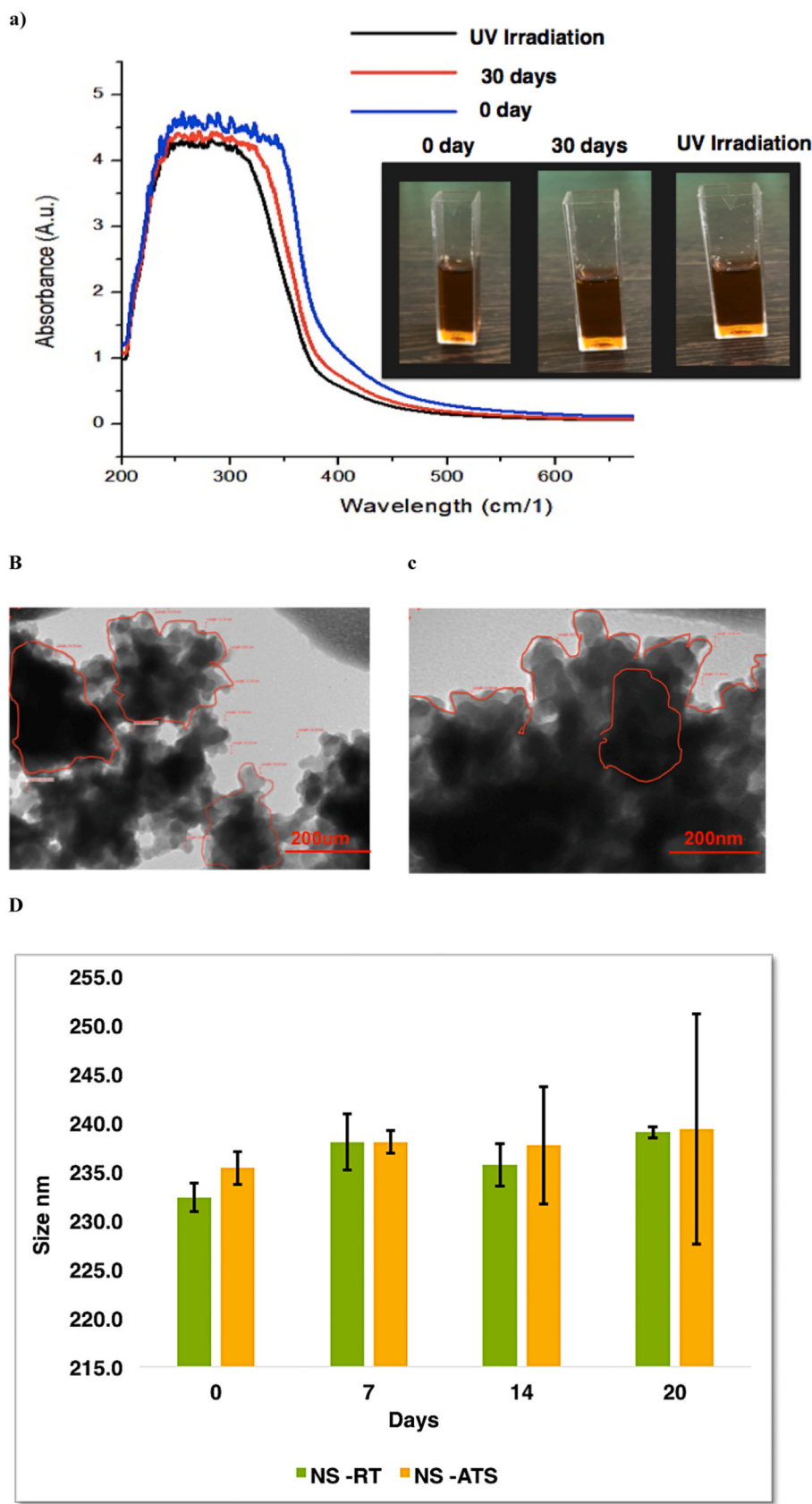
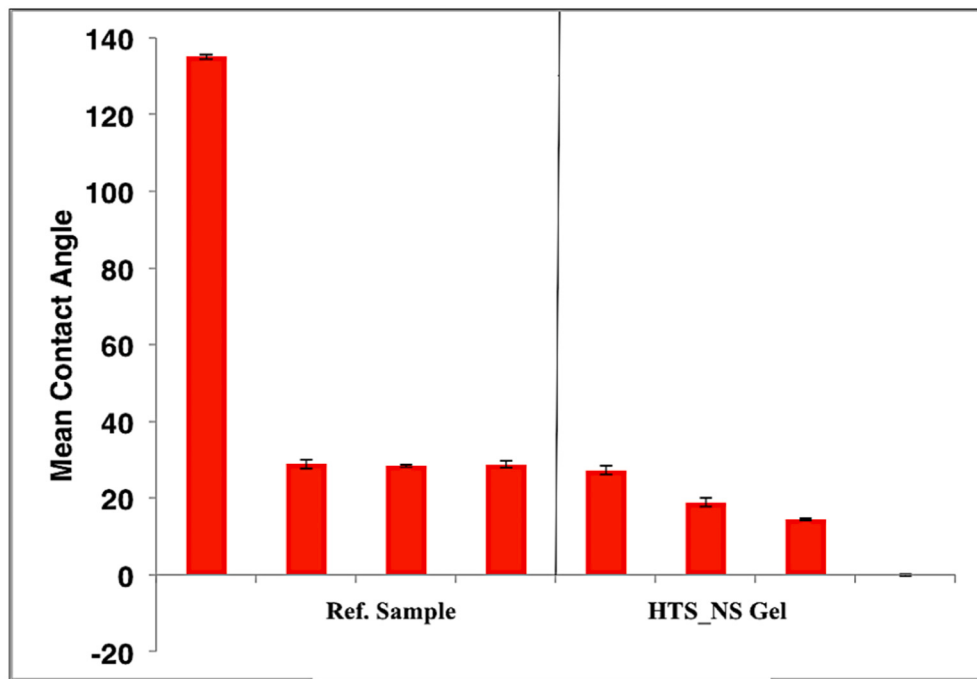


Fig. 6. a) Degradation state of HTS_NFG after UV spectra Initial, after storage at ambient temperature and after UV exposure and. TEM micrographs b) after storage and c) after UV Irradiation. d) Particle size of HTS_NFG during storage at ambient (RT = Room Temperature) temperature and 45 °C (ATS = Accelerated temperature study). Bars show standard deviations for n = 3 at significant level ($p > 0.05$).

a)



B

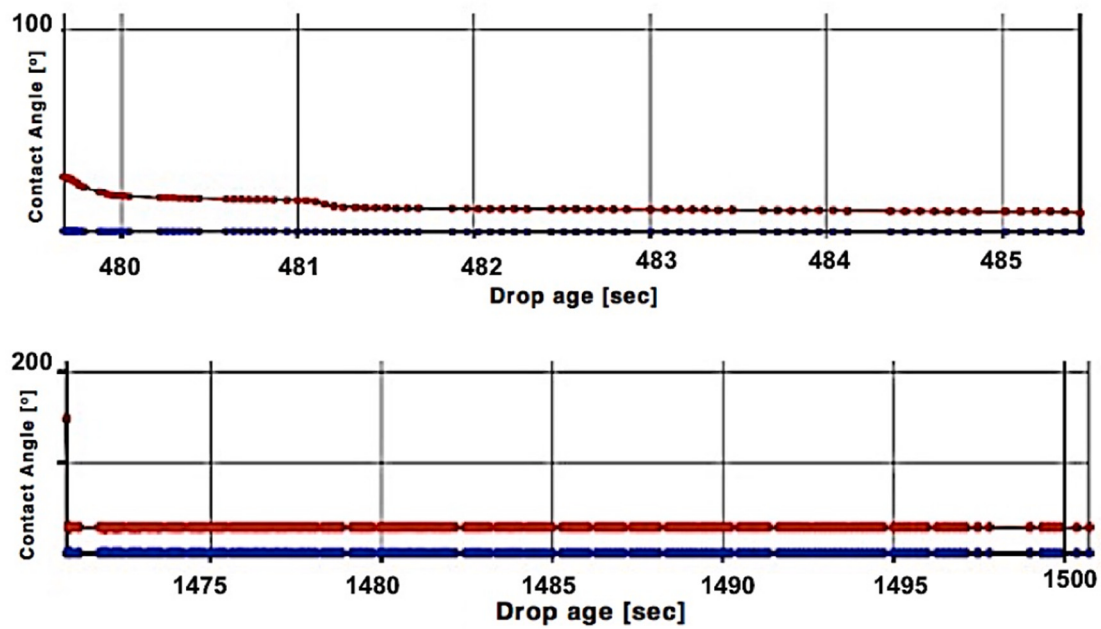


Fig. 7. a) Contact angle measurements. Bars show standard deviations for $n = 3$. Bars show standard deviations at significant level ($p < 0.05$). b) Contact angle vs. Drop age in HTS_NG sample (above) and reference sample (below). c) Droplet produced on leaf surface and its behavior (HTS_NS and Reference sample). d) Microscopic image of spreading behavior of HTS_NG (Red Dye was added for visualization). (For interpretation of the references to colour in this figure legend, the reader is referred to the web version of this article.)

be a good candidate for spray applications due to their ability to become thickened and sticky at high shear.

Rheological parameters were also measured by variation of storage modulus (G), loss modulus (G''), and complex viscosities (G). Fig. 5c

represents frequency sweep test of HTS NS showed that loss modulus G'' was lower than storage modulus G' . Storage modulus measures how much structure is present in a material and how much energy is stored in the elastic structure of the sample. The decrease in loss modulus

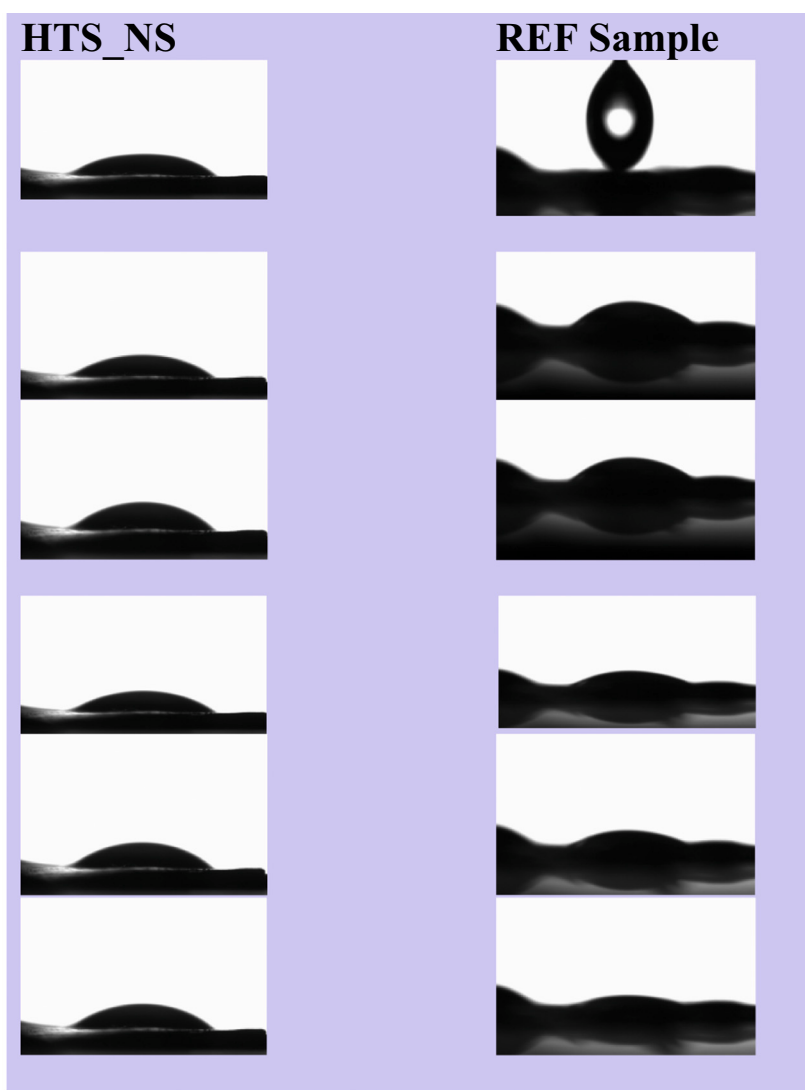
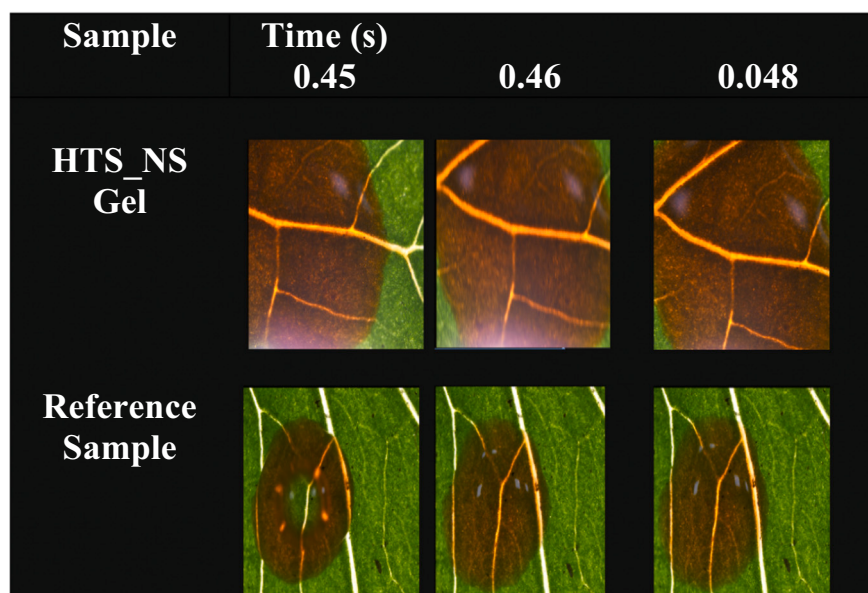
c**d**

Fig. 7. (continued).

decrease of HTS_NFG is due to its elastomer nature; a similar result was reported by the results of Houben et al. (2010) [51]. The results indicate that the NFG is more elastic than viscous, the elastic properties are desirable for spray applications as it can help prevent dripping or running. Overall, the rheological analysis highlights the potential of NFG to improve the performance and efficiency of spray applications in agricultural fields.

3.6. Metabolite investigations of HTS

The GC-MS analysis of HTS provided a comprehensive understanding of the volatile components present in it. The detailed methodology is provided in Supplementary Text 2. The retention index identification was done to correctly identify the chemical by comparing it to tabulated values of standards alkane ran under identical conditions using Kováts' retention index approach, which uses straight-chain alkane standards, is the most used [52]. The compounds identified from HTS are represented in a heat map (Supplementary Fig. 2 a). The HTS analysis identified 41 different compounds, representing 100 % of the total extract. The main constituents detected were Methyl elaidate (35.42 %), Ethyl Linolate (28.06 %), steric acid methyl ester (6.02 %), including several minor compounds such as fatty acid methyl ester represented in table (Supplementary Table 3). In a previous report a fungal biomass characterized by GC-MS showed the presence of fatty acid methyl ester [53]. These compounds present in the HTS might be potentially bioactive and could be further investigated for their biological effects. The diversity of compounds present in the extract suggests a complex chemical profile with various potential applications in agriculture.

LC-MS analyses of HTS were carried out to identify nonvolatile constituents of HTS. While entomopathogenic fungi infecting insects have been the source of many new and biologically active metabolites [54], insecticidal compounds have been found in metabolites of various fungi. The compounds identified from HTS are represented in a heat map (Supplementary Fig. S2b). The insecticidal compounds present in HTS can be classified into peptides, alkaloids, and others [55]. The significant compounds categorized as amino acids include betaine, L-phenylalanine, proline, and L-histidine were detected in HTS. In a previous report, the Entomopathogenic fungus displayed the presence of several amino acids [45], and these naturally occurring amino acid derivatives display significant activities against weeds, fungi, and insects [56]. In the present analysis of the HTS, P-Cyclophane, an important compound, was also detected in the HTS. According to the previous report P-Cyclophane is present in the Hirsutellone family and has wide range biological activities [57,58]. The results of the finding indicate that the presence of naturally occurring amino acid derivatives and hirsutellones (P-cyclophane) in the entomopathogenic fungus have promising potential for use in agricultural applications due to their excellent biological activity and effectiveness in pest and weed control [58]. The spectra of the compounds identified are given in Supplementary Fig. S3, and the list of compounds identified is given in Supplementary Table S4. The primary metabolites, their structural nature, and toxicity are reviewed in Table 2.

Table 3

Leaf retention and LR_s of the HTS_NS (\pm = S.E.: Standard error. Means (\pm S.E.) followed by the same letters (a-c) within LR % columns indicates significant difference ($p < 0.05$) at 5 % (Duncan's multi-range test).

	R1 (mg/cm ²)	R2 (mg/cm ²)	LR (%)
HTS_NS with chitosan+ silica	2.5 ± 0.22a	1.17 ± 0.71a	53.2 ± 0.54c
HT_NS with silica	2.9 ± 0.35a	0.9 ± 0.62a	68.9 ± 0.35b
Ref Sample	3.2 ± 0.12a	0.5 ± 0.06a	83.7 ± 2.1a

3.7. Stability storage and degradation patterns under UV light

The degradation caused by UV radiation in natural environments poses a substantial challenge to the long-term efficacy of bio-pesticides. Simulation study was undertaken to evaluate the UV resistance of HTS_NFG by exposing it to UV radiation and during storage through UV-visible spectrometry. In the UV irradiation test for 8 h and storage stability test (30 days) at an ambient temperature, the result of UV-visible spectra demonstrates that the self-assembly of NFG provides UV protection to HTS. Following UV irradiation and after storage at ambient temperature (Fig. 6a), no variation in absorbance was observed. Furthermore, the physical status and morphology of the NFG do not change, thus forming a higher compatibility state with HTS (Fig. 6a, b, and c). While storing at ambient temperature nanoparticle agglomeration likely stopped due to the restriction of accelerated particle movement, which could be brought by MNS surfactant in combination with CH and silica, preventing the formation of larger aggregates. Furthermore, nano-sized particles avoid creaming and settling, hence ensuring adequate long-term stability in nano systems [59]. There was a slight increase in the mean particle size after 30 days of storage, despite the slight particle growth; the size of NFG was retained in the nano range (Fig. 6d). Further, the results of mean particle size of NFG during storage at ambient temperature and 45 °C are non-significant ($p > 0.05$). The reason for maintaining size in the nano range was attributed to the combined effects of surfactants, silica, CH, and the optimized process of high-pressure homogenization. Thus, a higher compatibility state of HTS in the NFG system will potentially result in improved UV protection and shelf life. Overall, the study indicates that the NFG effectively enhances the UV resistance of HTS, making it a promising delivery system for applications requiring protection against UV exposure. These results suggest that incorporating HTS into NFG formulations could improve their durability and performance in outdoor or UV-exposure environments.

3.8. Wetting-spreading characteristics and drop spreading dynamics

Hydrophobic cabbage leaves were selected to evaluate the wettability behavior of HTS_NFG. The contact angle was a vital criterion to assess the hydrophilic and hydrophobic properties of the formulations [60,61]. As shown in Fig. 7a, the contact angle of the reference sample on the cabbage leaf surface was 120°, indicating the hydrophobic characteristic of the cabbage leaf [62]. Meanwhile, the contact angles on cabbage surfaces decrease constantly with time and drop to 28°. On the contrary, the contact angle of HTS_NFG produced on a cabbage leaf was 20° initially and dropped down continually, reaching 9°. The lower contact angle of HTS_NFG produced on the leaf decreased, and its constant decrease indicated that the HTS_NFG was easier to spread and wet on the leaf surface [63], which led to an enhancing wettability and spreading performance on a hydrophobic surface, the statement was supported by previous findings [53]. The results of contact angle behavior with drop-age were significantly difference among NFG and reference sample ($p < 0.05$). The contact angle of the droplets fluctuates over time as shown in Fig. 7b, showing dynamic wetting behavior. This information of contact angle measurement provides an understanding of the surface characteristics of the HTS_NFG droplets and their interactions with the leaf surface. Fig. 7c also shows the actual droplets that develop on the leaf surface, enabling visual inspection of their distribution. These pictures can aid in understanding how droplets interact with the microstructure of the leaf and possibly impact processes, such as spreading behavior, which is also presented in Fig. 7d.

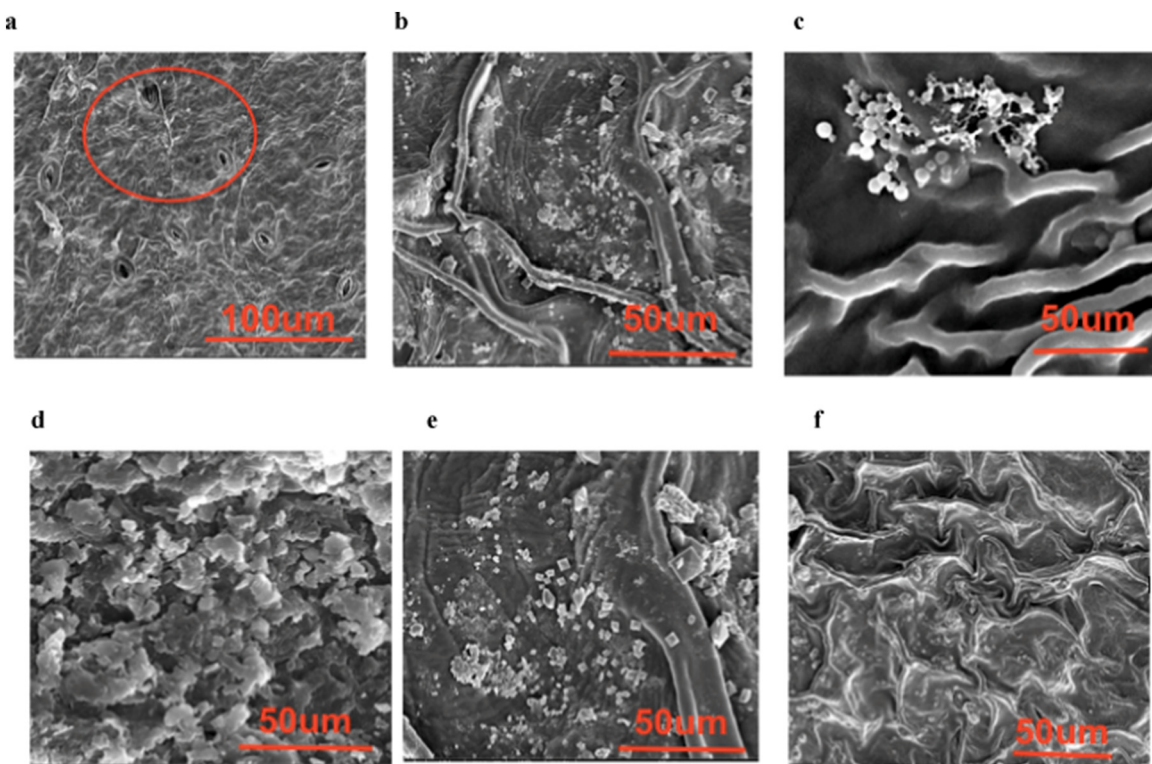


Fig. 8. Deposition properties of HTS_NS (Red circle showing stomata). (For interpretation of the references to colour in this figure legend, the reader is referred to the web version of this article.)

3.9. Deposition properties of HTS_NFG

The degree of resistance of the pesticide to washing off is a critical factor in determining the retention of the foliage spray in the leaf [62]. Initially, R1 leaf retention (HTS_NFG) and R2 leaf retention (Reference sample) in water were almost identical; however, R2 leaf retention of reference decreased after washing with water, while HTS_NFG retention was higher. The overall loss rate (LR%) for HTS_NFG was found to be

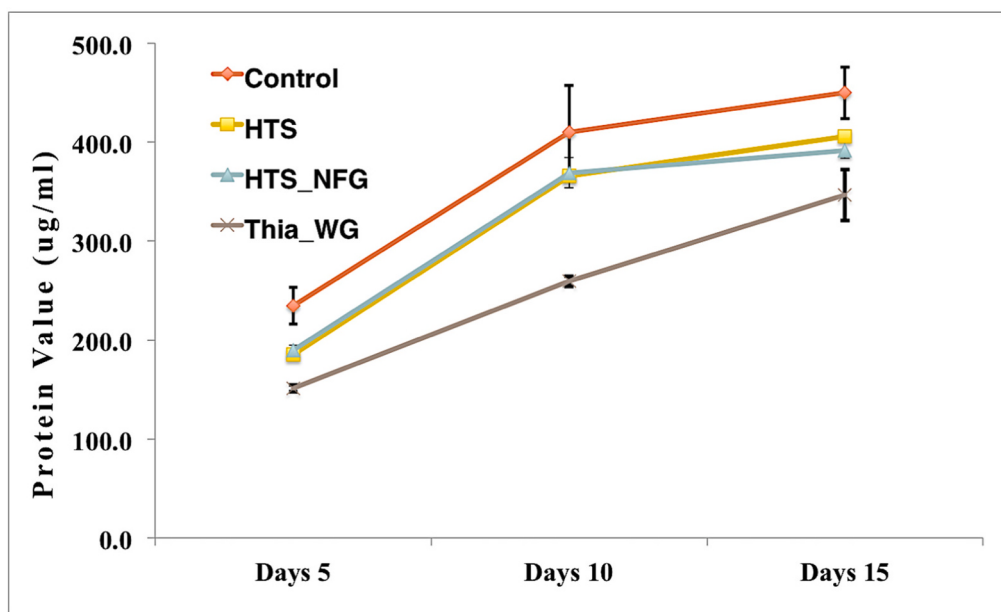
lowest in the presence of CH, and it was also lower than the Reference sample (Table 3). The results of the loss rate were significant ($p < 0.05$) among three treatments; with the minimum biopesticide loss in NFG with $53.2 \pm 0.54\%$. These results indicate that the HTS in NFG might be more resistant to washing off than the reference sample. Thus, we can infer that HTS_NFG exhibits superior crop leaf retention in the presence of CH compared to the reference sample. The enhanced retention properties can be due to the CH, which has been described as a

Table. 4

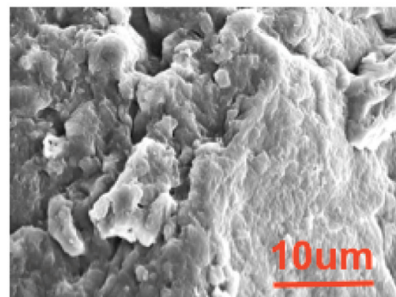
Effects of HTS_NFG mean aphid population on two different spice crops in an on-station experiment at the National Research Center on Seed & Spices, Ajmer India (November 2020 to February 2021), ($n = 3$) Control = Reference sample. ($S.E.m = \text{Standard Error of mean}$) CD = Critical difference 0.05 *square root transformation ($\sqrt{+/-}$).

S-no	Treatments	Aphids population					
		Before spray	After 1st spray			After 2nd spray	
			3 day	6 day	9 day	3 day	6 day
Crop-coriander							
1	H. T. 1.4 NFG (0.01 %).	124.3	54.4 (7.38)*	38.2 (6.25)	1.3 (1.60)	18.6 (4.42)	8.0 (2.99)
2	Control	154.1	120.6 (11.00)	116.4 (10.82)	124.1 (11.17)	180.2 (13.44)	113.9 (10.70)
	CD(0.05)		1.850	0.799	0.631	0.500	0.569
	S.E.m±		0.623	0.269	0.212	0.168	0.191
	Thiomethoxam –0.025 %	43.44	0.78	0.00	0.00		0.193
Crop-cumin							
1	H. T_NFG 1.4 NS (0.01 %).	69.7	60.3 (7.82)	27.3 (5.31)	19.0 (4.47)	11.0 (3.46)	8.0 (2.99)
2	Control	102.0	107.0 (10.37)	159.0 (12.63)	165.0 (12.86)	89.0 (9.47)	55.0 (7.47)
	CD at 5 %-		0.658	0.510	0.456	0.333	0.254
	SE.m (+/-)						0.571
	Thiamethoxam 0.025	43.56	19.00	15.78	13.56		

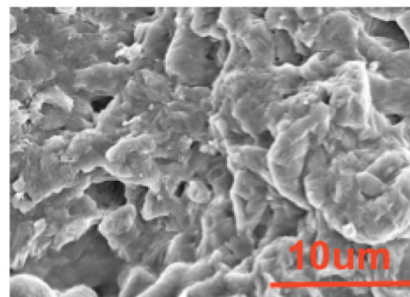
a



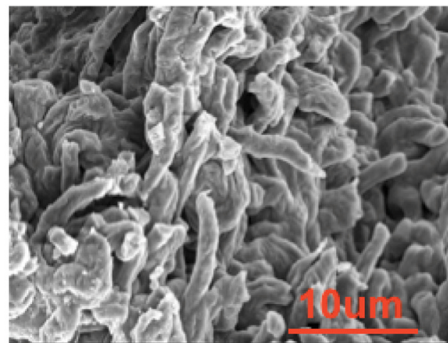
b



c



d



e

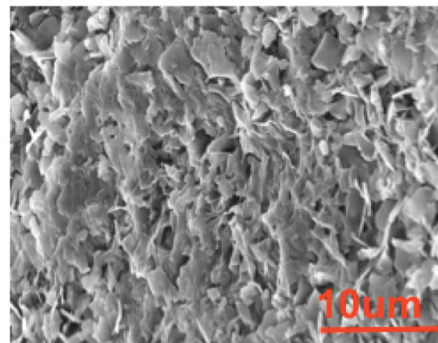
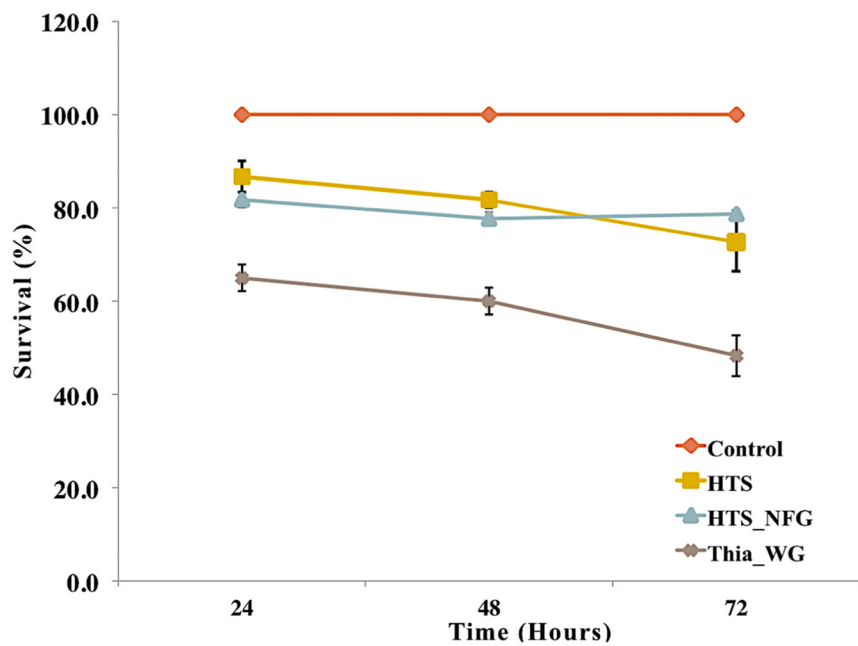


Fig. 9. Safety evaluation of HTS_NFG a) Effect of HTS_NFG on *Chlorella vulgaris* growth kinetics estimated via protein content Bars show standard deviations for n = 3 at significant level ($p < 0.05$). b-e) SEM images of *Chlorella vulgaris* surface after treatment on 15th day (b- control, c-HTS, d- HTS_NFG, e-Thia_WG) f) Percentage survival of *Artemia salina* shrimp incubated HTS_NFG for 72 h. Bars show standard deviations for n = 3 at significant level ($p < 0.05$). g) Microscopic images showing morphological changes in *Artemia salina* embryos between control, reference sample, unformulated HTS and HTS_NFG at 24, 48, and 72 h time interval. (EM – Embryonic membrane, HM- Hatching membrane, LB = limb buds pair 1 and 2, showing normal development.) (Magnification 10 \times).

f



g)

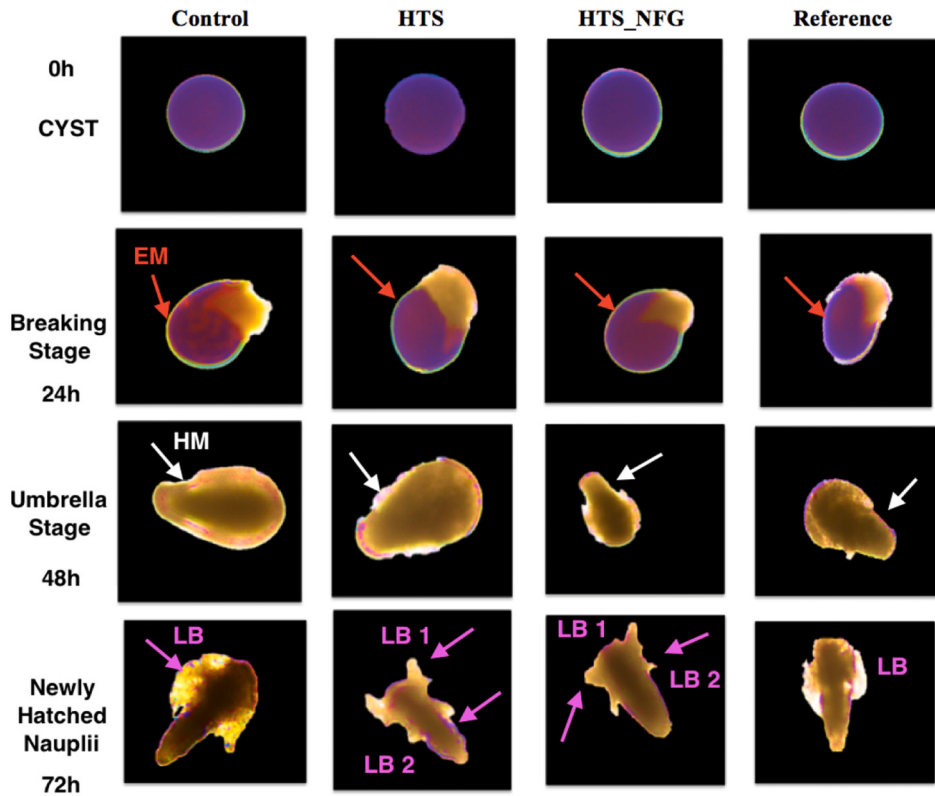


Fig. 9. (continued).

rainfastness agent [17], and the continuous phase glycerol, which functions as an additive. Additionally, the dispersion agents and the nano-sized particles further amplify this trait; a previous study has shown that the nano-sized particles hold great potential for improving the performance of pesticides against wash off [16]. The surface

morphology of leaves also confirmed the foliage adhesion performance in the succeeding experiment, as shown in Fig. 8. We examined and demonstrated the surface morphology of the blank cabbage leaf using SEM; the stomata were easily visible on the surface of the leaf (Fig. 8a). A distinct-shaped particle was observed after spraying the leaf with the

reference sample (Fig. 8b). However, upon washing, a few particles of the reference sample were present on the leaves (Fig. 8c). In contrast, in HTS_NFG, distinct particles were present pre-wash (Fig. 8d) and observed post-wash more dense in the presence of CH (Fig. 8e) compared to that without CH (Fig. 8d), these results suggest that HTS_NFG is more resistant to washing compared to the reference sample (RS). This difference is due to the low binding capacity of RS on the leaf surfaces, whereas in HTS_NFG glycerol serves as an additive, and nano flower framework conjugation between silica-CH and glycerol, improves the deposition properties of HTS_NFG, moreover, CH has been reported as a rainfastness adjuvant [24]. The significantly superior adhesion performance of NFG compared to commercial formulations suggests that NFG could potentially expand its application efficiency and reduce the amount of product required to attain effective results, achieving longer-lasting effects, lessening the need for frequent reapplication. Additionally, the enhanced adhesion properties of NFG could lead to reduced runoff, resulting in least wastage. This suggests that using NFG may not only improve efficacy but also contribute to more sustainable agricultural practices.

3.10. Field bioassay of HTS_NFG

Infield bioassays, the HTS-loaded NFG significantly reduced the aphid population with Critical difference of 0.05. Table 4 presents the results of the insecticidal bioassay in terms of aphid populations before and after the spray. In the trial conducted in 2021, the efficacy of HTS_NFG against aphids was evident from 3rd day following the initial spray and persisted until the 9th day. The bio-efficacy against aphids, after treatment with the NFG, showed a decrease in aphid population in coriander from the initial aphid population of 124.3 reduced to 54.4 on the 3rd day, 38.2-6th day, 1.3-9th day. In another crop, cumin, the population reduced decreased by half, from 67.7 to 27.3 on the 6th day and further decreased to 19 on the 9th day. Both crops showed a similar pattern after the second spray application. The control demonstrated a rise in the aphid population. The effectiveness was similar to the reference sample. The high efficacy of NFG is supported by multiple components in the HTS. The chemical profile of the substances, such as methyl esters and hydrocarbons, has revealed their insecticidal properties [63,64]. Furthermore, prior studies have demonstrated that amino acids and p-cyclophane derived from EPF fungi have noteworthy efficacy in controlling weeds, fungi, and insects [54,55]. The findings obtained from the field effectiveness of NFG indicate that it may be used as a successful method for delivering biopesticides. Overall, the NFG demonstrates potential as a viable solution for pest management in agriculture.

3.11. Safety assessment on non-target

Fungal biocontrol agents (BCAs) have been marketed to control crop pests and diseases. However, BCAs may produce toxic metabolites, whose presence in the formulated products, crops, and the environment should be considered along with the associated risk [8]. Further toxicity of the nanoparticles can have a significant impact on aquatic ecosystems [40]; therefore, the HTS_NFG was tested on higher concentrations on *Chollera* algae (growth kinetics and morphology alteration) and *Artemia salina* (Acute and developmental toxicity) (100 µg/L) as per previous reference [8]. The results showed that the nanoparticles had no significant negative effect on the growth kinetics and morphology of *Chollera* algae. Additionally, there was evidence of acute and developmental toxicity in *Artemia salina* at the tested concentration of 100 µg/L, which showed no significant toxicity. The results and discussion of the toxicity investigations are detailed below, under the subsequent headings.

3.12. Bio-toxicity studies on micro-algae: growth kinetics and morphology alteration

3.12.1. Growth Kinetics of algae culture

Algae are one of the most commonly used model organisms for toxicity studies of a toxicant. *Chlorella vulgaris* is one of the aquatic organisms most affected by pesticides, as Bedil et al. 2017 [65] demonstrated. To assess the toxicity of the green algae *Chlorella* spp., we tested it with HTS_NFG, algal development was monitored over 15 days, and the growth kinetics of the algal growth under the treatments were estimated. The treatment did not significantly reduce the algae growth rate or protein content in liquid cultures (Fig. 9a). Effect of HTS_NFG on *Chlorella vulgaris* growth kinetics estimated via protein content show significant level ($p < 0.05$). However, the growth kinetics analysis indicated that Thia-WG treated algae had a greater decrease in protein content and could be more toxic than HTS-NFG; however, HTS-NFG was just as safe as untreated HTS. These findings indicate that Thia-WG may exhibit more toxicity towards *Chlorella* spp. than HTS-NFG; however, HTS-NFG is still a viable choice for promoting algae development without adverse effects. In the previous report, nanoparticles exerted toxicity to the algal cells; however; it was shown that the nanoparticles toxicity was found to be dosage-dependent, with higher concentrations resulting in a greater number of interactions [40]. The lower toxicity of HTS-NFG compared to Thia-WG may be attributed to the amino acids (Table 2), which were found non-toxic to non-targets and the lower concentration.

3.12.2. Morphology alteration of algae after treatment

SEM imaging shows algal cell morphological changes after exposure and demonstrates effects on Algal cells (Fig. 9b-e). The control micrograph shows algal cells with a flat, non-destructive cell surface. Algal cells treated with unformulated HTS and HTS_NFG show similar morphological changes to the control. Thia is more toxic to algae cells with different morphologies bearing broken, shattered structures than the other two treatments and control. The toxicity of different treatments may vary depending on the specific active component and its mechanism of action. The Thia-WG-based system, in which Thia is easily accessible to the algae, might potentially result in further cellular harm. Previous research has demonstrated that the detrimental effects following exposure to nano particles lead to the cell membrane damage and cell lysis in the algal cells. Additionally, the diminished availability of nutrients contributes to the interrupted growth in algae [40]. The encapsulation of HTS in NFG might reduce aquatic toxicity by obstructing direct interaction between the HTS and aquatic species. Moreover, the free metabolites like amino acids detected in HTS (Table 2) were least toxic to the aquatic organisms [8], and the nano-assembled HTS did not impart modification in the morphology of algae, which suggests that the fungus metabolites in the presence of additives assembled in the nano range are non-toxic to the microalgae.

3.12.3. Microcrustacean (*Artemia salina*) bioassay: acute toxicity and development of *Artemia salina*

The biotoxicity of HTS_NFG has been investigated concerning its effects on *Artemia Salina*. *Artemia Salina* shrimps' survival rate diminishes proportionally with time, as seen in Fig. 9f. Percentage survival of *Artemia salina* shrimp incubated with HTS_NFG for 72 h shows a significant level ($p < 0.05$) among different treatments. Nevertheless, the findings of this investigation indicate that the HTS-NFG can successfully reduce the harmful effects on non-target species, which may be attributed to the presence of harmless bio-actives detected in the HTS [8]. *Artemia salina* had a higher survival rate compared to Thia WG. The results obtained for *Artemia salina* were also in line with the non-toxic properties of HTS in its nanoformulation. This study examined malformation and deformity endpoints to assess the developmental toxicity of HTS_NFG in *Artemia salina* embryos at the dose 100µg/L. The deformity analysis revealed that embryos exposed to 100 µg/mL HTS_NFG

Table 5

Phytotoxicity assessment of HTS_NFG (\pm = S.E.: Standard error. Means (\pm S.E.) followed by the same letters (a-c) within columns indicate no significant difference ($p > 0.05$) at 5 % (Duncan's multi-range test).

Crop	Treatments	Radicle (cm)	Plmule (cm)
Coriander	Control	2.60 ± 0.16a	0.21 ± 0.05a
	HTS NS	2.41 ± 0.15a	0.25 ± 0.18a
Cumin	Control	3.53 ± 0.51a	0.19 ± 0.05a
	HTS NS	2.93 ± 0.23a	0.19 ± 0.021a

exhibited morphological characteristics that were comparable to those of untreated embryos (Fig. 9g). There were no abnormalities detected during the developmental phases of any treatments, indicating that the concentration of HTS_NFG utilized in the study did not have a substantial effect on the development of *Artemia salina* embryos. Additional investigation is required to ascertain whether increased levels of HTS_NFG might lead to abnormalities or whether other variables contribute to developmental harm. The successful emergence of Nauplii from the embryos demonstrates that the concentration of HTS_NFG utilized in the study did not impede their development. The results of the biotoxicity studies suggest that NFG can serve as an effective vehicle for delivering biopesticides. In a nutshell, the NFG offers an intriguing and sustainable solution for agricultural pest management.

3.13. Seed germination potently test

The non-phytotoxic effect of HTS NS gel was assessed on the emergence of radicals and plumules from coriander and cumin seeds, depicted in Table 5. The 100 % coriander and cumin seed germination was observed in all sets after treatment with HTS_NFG gel at 48 h of exposure. The results of plumule and radical growth were non-significant ($p > 0.05$). The results indicate that the HTS NS gel does not negatively impact the germination process of coriander and cumin seeds. In previous study, nanoparticles shows similar compatibility towards rice seeds [35]. This implies that the gel is safe to use without compromising seed emergence. The HTS_NFG gel's compatibility with coriander and cumin highlights the formulation's non-phytotoxic nature.

4. Conclusions

In summary, we reported a glycerol-silica-CH-based system that can provide an improved dispersion of HTS in continuous phase and act as a vehicle for their enhanced bio-pesticide delivery. To overcome the issue of UV sensitivity of HTS, we loaded it in nanoscale suspension gel, attaining a flower shape. The HTS-loaded nanosuspension was formed by co-assembling MNS and fungal biomass in the glycerol medium and silica-CH following high shear mixing at 5000 RPM (ambient temperature), followed by HPH at pressure 600 bars five cycles each 2 per minute. The HTS-loaded NFG exhibited stability against UV and long-term storage due to the formation of a mechanically robust coating of silica and CH particles in the continuous medium. The process was successfully scaled up at the pilot level. The lower contact angle and non-significant toxicity to *Chlorella spp* algae and *Artemia salina* makes HTS_NFG a perfect candidate for use in agricultural applications. Moreover, the field bioassay on natural settings demonstrated that the HTS-loaded NFG vehicle exhibited effectiveness similar to commercial insecticide formulation. From the viewpoint of adhesion performance and wetting-spreading characteristics, HTS_NFG exhibited good efficiency for foliar delivery. The results obtained in this study highlight that our NFG could be used as a useful vehicle for delivering HTS.

CRediT authorship contribution statement

Smriti Kala: Writing – original draft, Methodology, Investigation,

Formal analysis, Conceptualization. **Chetan Jawle:** Investigation. **Mangesh AshokRao Pande:** Methodology. **Amrish Agarwal:** Supervision. **Krishna Kant:** Methodology. **B.K. Mishra:** Methodology. **Mukesh Kumar Singh:** Methodology. **L.K. Takhur:** Resources.

Declaration of competing interest

The authors declare no conflict of interest.

Appendix A. Supplementary data

Supplementary data to this article can be found online at <https://doi.org/10.1016/j.ijbiomac.2024.137476>.

Data availability

All the data is shown here.

References

- [1] Azza A. Elbanhawy, Elsherbiny A. Elsherbiny, Ahmed E. Abd, Gamal M. El-Mageed, Abdelfattah, Potential of fungal metabolites as a biocontrol agent against cotton aphid, *Aphis gossypii* Glover and the possible mechanisms of action, *Pestic. Biochem. Physiol.* 159 (2019) 34–40.
- [2] K.S. Akutse, J.W. Kimemia, S. Ekesi, F.M. Khamis, O.L. Ombura, S. Subramanian, Ovicultural effects of entomopathogenic fungal isolates on the invasive fall armyworm *Spodoptera frugiperda* (Lepidoptera: Noctuidae), *J. Appl. Entomol.* 00 (2019) 1–9.
- [3] Chen Zhang, et al., Metabolic responses of *Beauveria bassiana* to hydrogen peroxide-induced oxidative stress using an LC-MS-based metabolomics approach, *J. Invertebr. Pathol.* 137 (2016) 1–9.
- [4] K. Kiran Kumar, et al., Microbial biopesticides for insect pest management in India: current status and future prospects, *J. Invertebr. Pathol.* 165 (2019) 74–81.
- [5] de la Cruz Quiroz, Reynaldo; Cruz Maldonado, Juan Jesús; Rostro Alanís, Magdalena de Jesús; Torres, J. Antonio; Parra Saldivar, Roberto. Fungi-based biopesticides: shelf-life preservation technologies used in commercial products. *J. Pest. Sci.*, 92, (2019) 1003–1015.
- [6] V.H. Vu, S.I. Hong, K. Kim, Production of aerial conidia of *Lecanicillium lecanii* 41185 by solid-state fermentation for use as a mycoinsecticide, *Mycobiology* 36 (2008) 183–189.
- [7] R. Alves, 003 SEB 8th Sincobiol 54 (2003) 42.
- [8] M. Favilla, et al., Toxicity assessment of metabolites of fungal biocontrol agents using two different (*Artemia salina* and *Daphnia magna*) invertebrate bioassays, *Food Chem. Toxicol.* 44 (2006) 1922–1931.
- [9] Douxin Xiao, et al., High foliar affinity cellulose for the preparation of efficient and safe fipronil formulation, *J. Hazard. Mater.* 384 (2020) 121408.
- [10] A.M.M. Sayed, R.W. Behle, Comparing formulations for a mixed-microbial biopesticide with *Bacillus thuringiensis* var. *kurstaki* and *Beauveria bassiana* blastospores, *Arch. Phytopathol. Plant Protect.* 50 (15–16) (2017) 745–760.
- [11] C.V. Patil, C.D. Patil, C.P. Narkhede, R.K. Suryawanshi, S.H. Koli, L. Shinde, B. V. Mohite, Photsynthesized gold nanoparticles-Bacillus thuringiensis (Bt-GNP) formulation: a novel photo stable preparation against mosquito larvae, *J. Clust. Sci.* 29 (4) (2018) 577–583.
- [12] P. Kumar, S. Pandhi, D.K. Mahato, M. Kamle, A. Mishra, Bacillus-based nano-bioformulations for phytopathogens and insect-pest management, *Egypt. J. Biol. Pest Control* 31 (2021) 128.
- [13] N. Arun Kumar, M. Deecaraman, C. Rani, Nanosuspension technology and its applications in drug delivery, *Asian J. Pharm.* 3 (3) (2009).
- [14] S.J. Lee, H. Jang, D.N. Lee, Inorganic Nanoflowers—synthetic strategies and physicochemical properties for biomedical applications: A review, *Pharmaceutics* 14 (2022) 1887.
- [15] J.L. López-Miranda, B.L.E. Sánchez, R. Esparza, M. Estévez, Self-assembly of ZnO nanoflowers synthesized by a green approach with enhanced catalytic, and antibacterial properties, *Mater. Chem. Phys.* 289 (2022) 126453.
- [16] J. Luo, Y. Gao, Y. Liu, et al., Self-assembled degradable Nanogels provide foliar affinity and pinning for pesticide delivery by flexibility and adhesiveness adjustment, *ACS Nano* 15 (9) (2021) 14598–14609.
- [17] P.K. Panda, K. Sadeghi, K. Park, J. Seo, Recent advances in poly (vinyl alcohol)/natural polymer based films for food packaging applications: A review food packaging and shelf, *Life* 33 (2022) 100904.
- [18] P.K. Panda, K. Sadeghi, K. Park, J. Seo, Regeneration approach to enhance the antimicrobial and antioxidant activities of chitosan for biomedical applications, *Polymers* 15 (1) (2023) 132.
- [19] Amel Mohamed Abouelnaga, A.M. Mansour, Ali B. Abou, Amany M. Hammad, El Nahrawy, Optimizing magnetic, dielectric, and antimicrobial performance in chitosan-PEG-Fe203@NiO nanomagnetic composites, *Int. J. Biol. Macromol.* 260 (2) (2024) 129545.
- [20] Amal M. Abouelnaga et al., Expansion of Nanosized MgSiO₃/Chitosan Nanocomposite Structural and Spectroscopic for Loading Veloset by Nanomaterial Intervention. (2021) *ECS J. Solid State Sci. Technol.* 10 121003.

- [21] M. Lavorgna, I. Attianese, G.G. Buonocore, A. Conte, M.A. Del Nobile, F. Tescione, E. Amendola, MMT-supported ag nanoparticles for chitosan nanocomposites: structural properties and antibacterial activity, *Carbohydr. Polym.* 102 (2014) 385–392.
- [22] Muhammad Asif Javaid, Rasheed Ahmad Khera, Khalid Mahmood Zia, Kei Saito, Ijaz Ahmad Bhatti, Muhammad Asghar, Synthesis and characterization of chitosan modified polyurethane bio-nanocomposites with biomedical potential, *Int. J. Biol. Macromol.* 115 (2018) 375–384.
- [23] R. Sánchez, G.B. Stringari, J.M. Franco, C. Valencia, C. Gallegos, Use of chitin, chitosan and acylated derivatives as thickener agents of vegetable oils for bio-lubricant applications, *Carbohydr. Polym.* 85 (2011) 705–714.
- [24] B.L. Symonds, C.I. Lindsay, N.R. Thomson, V.V. Khutoryanskiy, Chitosan as a Rainfastness Adjuvant for Agrochemicals, *RSC Adv.*, 2016.
- [25] Philippa D. Darbre, Introduction to personal care products, in: *Personal Care Products and Human Health*, Academic Press, 2023, pp. 3–31.
- [26] Gürgen, Selim; Kuşhan, Melih Cemal; Li, Weihua. Shear thickening fluids in protective applications: A review. *Prog. Polym. Sci.*, 75 (2017), 48–72.
- [27] Amany Mohamed Elnahrawy, Yong Soo Kim, Ahmed I. Ali, Synthesis of hybrid chitosan/calcium aluminosilicate using a sol-gel method for optical applications, *J. Alloys Compd.* 676 (2016) 432–439.
- [28] Saira Bibi, Arifa Jamil, Tariq Yasin, Muhammad Aftab Rafiq, Mohsan Nawaz, Gareth J. Price, Ultrasound promoted synthesis and properties of chitosan nanocomposites containing carbon nanotubes and silver nanoparticles, *Eur. Polym. J.* 105 (2018) 297–303.
- [29] CIPAC method, MT 177. © 2022 CIPAC - Collaborative International Pesticides Analytical Council.
- [30] C.-P. Chin, H.-S. Wu, S.S. Wang, New approach to pesticide delivery using Nanosuspensions: research and applications, *Ind. Eng. Chem. Res.* 50 (12) (2011) 7637–7643.
- [31] Z. Pan, B. Cui, Z. Zeng, L. Feng, G. Liu, H. Cui, H. Pan, Lambda-Cyhalothrin nanosuspension prepared by the melt emulsification-high pressure homogenization method, *J. Nanomat.* 16 (2015) 263.
- [32] A. Chindrus, D. Copot, C.-F. Caruntu, Predictive control strategy for continuous production systems: A comparative study with classical control approaches using simulation-based analysis, *Processes* 11 (4) (2023) 1258, <https://doi.org/10.3390/pr11041258>.
- [33] L. Alison, P.A. Rühs, E. Tervoort, A. Teleki, M. Zanini, L. Isa, A.R. Studart, Pickering and Network stabilization of biocompatible emulsions using chitosan-modified silica nanoparticles, *Langmuir* 32 (50) (2016) 13446–13457.
- [34] P. Chu, H. Zhang, F. Chen, Z. Zhang, Rheological behaviors of nanosilica suspensions with different dispersion levels prepared by the bead milling technique, *Compos. A: Appl. Sci. Manuf.* 81 (2015) (2016) 34–40.
- [35] J. Feng, J. Yang, Y. Shen, W. Deng, W. Chen, Y. Ma, S. Dong, Mesoporous silica nanoparticles prepared via a one-pot method for controlled release of abamectin: properties and applications, *Microporous Mesoporous Mater.* 311 (2021) 110688.
- [36] S. Appah, H. Zhou, P. Wang, M. Ou, W. Jia, Charged monosized droplet behaviour and wetting ability on hydrophobic leaf surfaces depending on surfactant-pesticide concentrate formulation, *J. Electrostat.* 100 (2019) 103356.
- [37] H. Qin, X. Zhou, D. Gu, L. Li, C. Kan, Preparation and characterization of a novel waterborne lambda-cyhalothrin/alkyd nanoemulsion, *J. Agric. Food Chem.* 67 (2019) 10587–10594.
- [38] S. Kala, C.K.D. Jawle, N. Sogan, A. Agarwal, K. Kant, B.K. Mishra, J. Kumar, Analogous foliar uptake and leaf-to-root translocation of micelle nanoparticles in two dicot plants of diverse families, *NanoImpact* 28 (1) (2022) 00431.
- [39] Bo Cui, Lei Feng, Zhenzhong Pan, Yu Manli, Zhanghua Zeng, Changjiao Sun, Xiang Zhao, Yan Wang, Haixin Cui, Evaluation of stability and biological activity of solid Nanodispersion of lambda- Cyhalothrin, *PLoS One* 10 (8) (2015) 1013595.
- [40] Pallavi Saxena, et al., Mechanism of nanotoxicity in *Chlorella vulgaris* exposed to zinc and iron oxide, *Toxicol. Rep.* 8 (2021) 724–731.
- [41] A. Shokry, M. Khalil, H. Ibrahim, et al., Acute toxicity assessment of polyaniline/ag nanoparticles/graphene oxide quantum dots on *Cypridopsis vidua* and *Artemia salina*, *Sci. Rep.* 11 (5) (2021) 336.
- [42] S. Das, V.K. Singh, Chaudhari Dwivedy, A.K., Upadhyay, Neha., Singh, Pallavi., Sharma, Sarika., Dubey, N.K., Encapsulation in chitosan based nanomatrix as an efficient green technology to boost the antimicrobial, antioxidant and in situ efficacy of *Coriandrum sativum* essential oil, *Int. J. Biol. Macromol.* 15 (133) (2019) 294–305.
- [43] E.O.M. Ali, N.A. Shakil, V.S. Rana, D.J. Sarkar, S. Majumder, P. Kaushik, B. Singh, J. Kumar, Antifungal activity of nano emulsions of neem and citronella oils against phytopathogenic fungi, *Rhizoctonia solani* and *Sclerotium rolfsii*, *Ind. Crop. Prod.* 108 (2017) 379–387.
- [44] D. Sharma, D. Maheshwari, G. Philip, R. Rana, S. Bhatia, M. Singh, R. Gabrani, S. K. Sharma, J. Ali, R.K. Sharma, S. Dang, Formulation and optimization of polymeric nanoparticles for intranasal delivery of lorazepam using box-Behnken design: in vitro and in vivo evaluation, *Biomed. Res. Int.* 2156010 (2014).
- [45] Salman et al. FTIR spectroscopy for detection and identification of fungal phytopathogenes. *Spectroscopy* 24 (2010) 261–267.
- [46] S. Sivakesava, J.M. Irudayaraj, C. Debroy, Differentiation of microorganisms by FTIR-ATR and NIR spectroscopy, *Trans. ASAE* 47 (2004) 951–957.
- [47] K. Dukor, *Handbook of Vibrational Spectroscopy*, Wiley, Chichester, UK, 2001.
- [48] N. Kumar, R.K. Salar, M. Prasad, K. Ranjan, Synthesis, characterization and anticancer activity of vincristine loaded folic acid-chitosan conjugated nanoparticles on NCI-H460 non-small cell lung cancer cell line, *Egypt. J. Basic Appl. Sci.* 5 (1) (2018) 87–99.
- [49] M. Wei, K. Lin, L. Sun, Shear thickening fluids and their applications, *Mater. Des.* 216 (2022) 110570.
- [50] M.C. Teixeira et al., D-a-tocopherol nanoemulsions: size properties, rheological behavior, surface tension, osmolarity and cytotoxicity, *Saudi Pharm. J.* (2017) 25; 31–35.
- [51] A. Houben, H. Götz, M. Mitzscherling, T. Becker, Modification of the rheological behavior of amaranth (*Amaranthus hypochondriacus*) dough, *Food Sci. Technol.* 51 (3) (2010) 350–356.
- [52] A. Marques Francisco De, J.S. Mcelfresh, Jocelyn G. Millar, Kováts retention indexes of monounsaturated C12, C14, and C16 alcohols, acetates and aldehydes commonly found in lepidopteran pheromone blends, *J. Braz. Chem. Soc.* 11 (6) (2000) 592–599.
- [53] N. Sogan, S. Kala, N. Kapoor, et al., Novel development of *Lecanicillium lecanii*-based granules as a platform against malarial vector *Anopheles culicifacies*, *World J. Microbiol. Biotechnol.* 39 (2023) 142.
- [54] Gerhard Lang, et al., Hirsutide, a cyclic tetrapeptide from a spider-derived entomopathogenic fungus, *Hirsutella sp.* *J. Nat. Prod.* 68 (2005) 1303–1305.
- [55] Sakuda, S., & Kimura, M. Toxins of microorganisms. *Comprehensive Natural Products II*, (2010) 411–455.
- [56] Wojciech Szajdak, Stanisław Balazy, Teresa Meysner, Amino acids in entomopathogenic fungi cultured in vitro lech, *Agronomy* 10 (2020) 1899.
- [57] Clemens Lamberth, Naturally occurring amino acid derivatives with herbicidal, fungicidal or insecticidal activity, *Amino Acids* 48 (4) (2016) 929–940.
- [58] Ohashi Masao, T.B. Kakule, M.C. Tang, C.S. Jamieson, M. Liu, Y.L. Zhao, K. N. Houk, Y. Tang, Biosynthesis of para-cyclophane-containing hirsutellone family of fungal natural products, *J. Am. Chem. Soc.* 21;143 (15):5605–5609 (2021).
- [59] L. Rigano, N. Lionetti, Nanobiomaterials in galenic formulations and cosmetics, *Nanobiomaterials in Galenic Formulations and Cosmetics* (2016) 121–148.
- [60] Masahiko Isaka, Wai Prathumpai, Patcharaporn Wongsa, Morakot Tanticharoen, Hirsutellone F, a dimer of Antitubercular alkaloids from the seed fungus *Trichoderma* species BCC 7579, *Org. Lett.* 8 (13) (2006) 2815–2817.
- [61] E. Spielman-Sun, A. Avellan, G.D. Bland, R.V. Tappero, A.S. Acerbo, J.M. Unrine, G.V. Lowry, Nanoparticle surface charge in uences translocation and leaf distribution in vascular plants with contrasting anatomy, *Environ. Sci. Nano* 6 (8) (2019) 2508–2519.
- [62] J. Yao, B. Cui, X. Zhao, et al., Preparation, characterization, and evaluation of azoxystrobin nanosuspension produced by wet media milling, *Appl. Nanosci.* 8 (2018) 297–307.
- [63] S.M. Samesh Soliman, B.Q. Saeed, S.A. Elseginy, F. Al-Marzoob, I.M. Ahmady, A. El-Kebway Ali, H. Rania, Critical discovery and synthesis of novel antibacterial and resistance-modifying agents inspired by plant phyto-chemical defense mechanisms, *Chem. Biol. Interact.* 335 (2021) 109318.
- [64] A. Purkait, S. Biswas, S. Saha, D.K. Hazra, Kusal Roy, P.K. Biswas, S.K. Ghosh, R. K. Kole, Formulation of plant based insecticides, their bio-efficacy evaluation and chemical characterization, *Crop Prot.* 125 (2019) 104907.
- [65] Burcin Bedil, A Kadri Cetin, Toxicity of four fungicides to the growth and protein amount Of *Chlorella Vulgaris* *Fresenius Environ. Bull.* (2017) 1778–1783.
- [66] Shuai Zhang, et al., The ecotoxicity and tribological properties of choline amino acid ionic liquid lubricants, *Tribol. Int.* 121 (2018) 435–441.
- [67] M. Shaaban, R.P. Maskey, I. Wagner-Döbler, H. Laatsch, Pharcine, a natural p-cyclophane and other indole derivatives from *Cytophagasp.* Strain AM13.11, *J. Nat. Prod.* 65 (11) (2002) 1660–1663.

Abbreviations

- CH:* Chitosan
HTS: *Hirsutella thompsoni* (HTS)
EPF: Entomopathogenic fungus
NFG: Nanoflower gel
MNS: Methyl naphthalene sulphonate
HPH: High Pressure Homogenization
Thia: Thiamethoxam
PG: Propylene Glycol